Cell Reports

Article

Kinetochore and ionomic adaptation to whole-genome duplication in *Cochlearia* shows evolutionary convergence in three autopolyploids

Graphical abstract

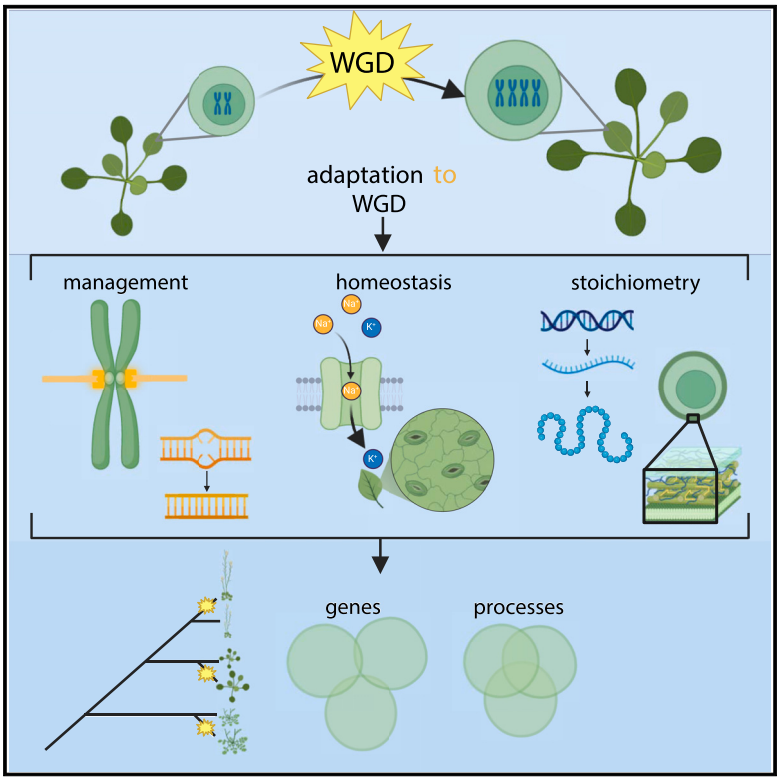

Authors

Sian M. Bray, Tuomas Hämälä, Min Zhou, ..., James D. Higgins, Marcus A. Koch, Levi Yant

Correspondence

levi.yant@gmail.com

In brief

Bray et al. identify selective sweeps on core kinetochore components following WGD, with the strongest signal of a selective sweep at the ortholog of a polyploid cancer target. Comparing three independently formed autopolyploid species, they detect low gene- but high process-level evolutionary convergence.

Highlights

- A suite of kinetochore components evolves in response to WGD in *Cochlearia officinalis*
- The strongest selection signal genome-wide is at *CENP-E*, a polyploid cancer target
- Broadly, DNA management and ion homeostasis processes evolve post-WGD
- Three independently formed autopolyploid species exhibit process-level convergent evolution

Bray et al., 2024, Cell Reports *43*, 114576
August 27, 2024
https://doi.org/10.1016/j.celrep.2024.114576

CellPress

Cell Reports

CellPress
OPEN ACCESS

Article

Kinetochore and ionomic adaptation to whole-genome duplication in *Cochlearia* shows evolutionary convergence in three autopolyploids

Sian M. Bray,[1,2] Tuomas Hämälä,[1,10] Min Zhou,[1,11,12] Silvia Busoms,[2,3] Sina Fischer,[1] Stuart D. Desjardins,[4] Terezie Mandáková,[5] Chris Moore,[1] Thomas C. Mathers,[6,13] Laura Cowan,[1,14] Patrick Monnahan,[2] Jordan Koch,[2] Eva M. Wolf,[7] Martin A. Lysak,[5] Filip Kolar,[8,9] James D. Higgins,[4] Marcus A. Koch,[7] and Levi Yant[1,8,15,*]

[1]The University of Nottingham, Nottingham NG7 2RD, UK
[2]The John Innes Centre, Norwich NR4 7UH, UK
[3]Department of Plant Physiology, Universitat Autònoma de Barcelona, 08193 Barcelona, Spain
[4]Department of Genetics and Genome Biology, University of Leicester, Leicester LE1 7RH, UK
[5]Central European Institute of Technology, Masaryk University, 625 00 Brno, Czech Republic
[6]Department of Crop Genetics, John Innes Centre, Norwich Research Park, Norwich NR4 7UH, UK
[7]Centre for Organismal Studies (COS), Heidelberg University, 69120 Heidelberg, Germany
[8]Department of Botany, Charles University, Benátská 2, 12801 Prague, Czech Republic
[9]The Czech Academy of Sciences, Zámek 1, 252 43 Průhonice, Czech Republic
[10]Present address: Production Systems, Natural Resources Institute Finland, Jokioinen 31600, Finland
[11]Present address: Department of Obstetrics and Gynecology, Women and Children's Hospital of Chongqing Medical University, Chongqing 401147, China
[12]Present address: China and Department of Obstetrics and Gynecology, Chongqing Health Center for Women and Children, Chongqing 401147, China
[13]Present address: Tree of Life, Welcome Sanger Institute, Hinxton, Cambridge CB10 1SA, UK
[14]Present address: Department of Plant Sciences, Cambridge University, Cambridge CB2 3EA, UK
[15]Lead contact
*Correspondence: levi.yant@gmail.com
https://doi.org/10.1016/j.celrep.2024.114576

SUMMARY

Whole-genome duplication (WGD) occurs in all kingdoms and impacts speciation, domestication, and cancer outcome. However, doubled DNA management can be challenging for nascent polyploids. The study of within-species polyploidy (autopolyploidy) permits focus on this DNA management aspect, decoupling it from the confounding effects of hybridization (in allopolyploid hybrids). How is autopolyploidy tolerated, and how do young polyploids stabilize? Here, we introduce a powerful model to address this: the genus *Cochlearia*, which has experienced many polyploidization events. We assess meiosis and other polyploid-relevant phenotypes, generate a chromosome-scale genome, and sequence 113 individuals from 33 ploidy-contrasting populations. We detect an obvious autopolyploidy-associated selection signal at kinetochore components and ion transporters. Modeling the selected alleles, we detail evidence of the kinetochore complex mediating adaptation to polyploidy. We compare candidates in independent autopolyploids across three genera separated by 40 million years, highlighting a common function at the process and gene levels, indicating evolutionary flexibility in response to polyploidy.

INTRODUCTION

Whole-genome duplication (WGD; leading to polyploidy) is a dramatic mutation that disrupts fundamental cellular processes.[1,2] Yet, for lineages that can adapt to a transformed polyploid state, it can hold great promise.[1–3] Across life's kingdoms, polyploidy is associated with speciation and adaptation, and in plants, polyploids are overrepresented among crops.[4] But despite its importance to evolution and agriculture, we do not yet know why some polyploids thrive while others do not.[2,5]

Understanding the diverse issues that face young polyploids may help us understand why some polyploids succeed while others fail. For polyploids originating from within-species genome doubling (autopolyploids), specific challenges emerge concerning DNA management. These involve the handling of the doubled complement of chromosomes, with the most obvious issues concerning chromosome segregation at meiosis.[6,7] In diploids, each chromosome has only a single homolog with which to engage in meiotic crossovers, but in an autotetraploid, there are three possible crossover partners for each chromosome, each roughly equivalent. Therefore, if a chromosome establishes multiple crossover events, then these might occur with more than a single other homolog, possibly resulting in breakage.[6,7] For between-species hybrid polyploids

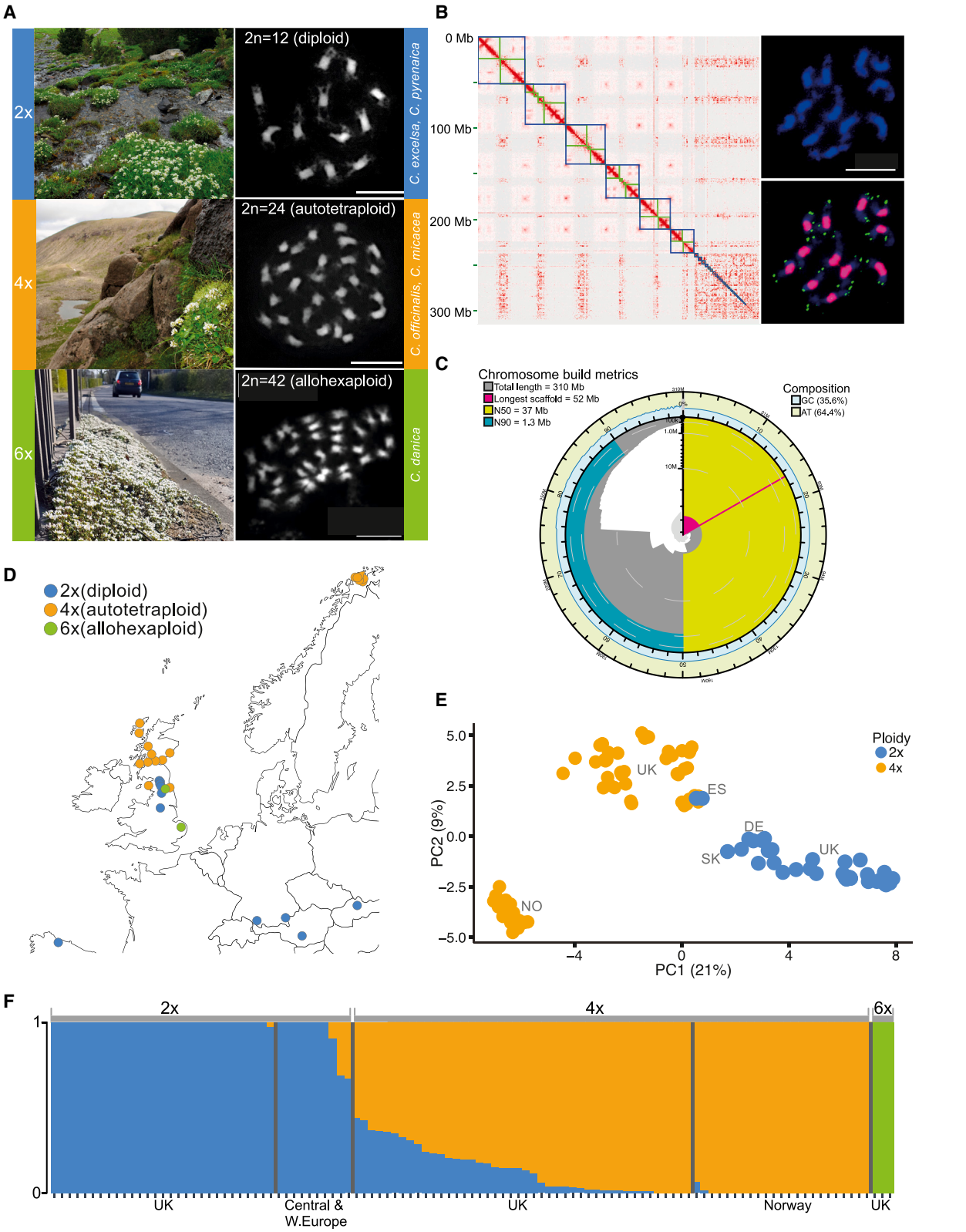

(legend on next page)

(allopolyploids, which combine genomes of two different diploid parent species), such events are much less of a problem because pairing partner preferences commonly restrict possible crossover events to the single most homologous chromosome from the same ancestral genome. Other changes are common across polyploids, such as "nucleotypic" factors that may affect a variety of fundamental cellular characteristics, including cell size, nuclear volume, and cell cycle duration, which can have profound effects on physiology.[5,8] Together, these novel changes resulting from polyploidy can have substantial phenotypic impacts on adaptation, e.g., through enhanced dehydration stress tolerance[9] and larger fruit and grain size.[10] However, given that these genetic and physiologic changes happen rather suddenly as genome complement increases, they may inhibit the establishment of nascent polyploids if adaptation to the new state is not rapidly achieved.[11] Nonetheless, successful autopolyploids persist in nature, indicating that early challenges can be overcome.

To date, work in two diploid-autotetraploid model systems has explicitly sought the basis of adaptation to autopolyploidy in young (<300,000-year-old) but stable lineages. However, there was little concordance between their results. First, in *Arabidopsis arenosa*, a handful of physically and functionally interacting meiosis proteins exhibit the strongest signals of selection in a young autopolyploid relative to diploid sisters.[12,13] Derived alleles of these genes directly decrease chromosome crossover rates, stabilizing autotetraploid meiosis.[14–17] Next, a study in *Cardamine amara* was performed to test whether the striking signal of adaptive evolution at meiosis proteins seen in *A. arenosa* might be recapitulated in an independent autopolyploid 17 million years diverged. However, the results of genome scans in *C. amara* showed no excess overlap in candidate orthologs with *A. arenosa* beyond the quantity expected by chance.[18]

These works gave some insight but were limited in their power to test whether there may be salient processes that commonly stabilize recent polyploids. In particular, in *C. amara*, only two diploid and two tetraploid populations were assayed by a low-coverage pool-seq approach, and the reference genome used was very fragmented.[18] Of greater biological significance, as noted by the authors of the *C. amara* study, widespread vegetative reproduction in *C. amara* likely offers a modicum of escape from selection for meiotic stability in the young autopolyploid, consistent with the observed results.[18] Thus, minimal convergence between these systems leaves unresolved whether there may be salient processes that commonly stabilize recent polyploids. This is important because the major genomic changes that occur in young polyploids may also help explain why some polyploids are so successful and some are not.

Here, we test in a robust system that closely parallels *A. arenosa* whether there may be common processes that stabilize these multiple, independent, and successful recently formed autopolyploids. Importantly, this system does not rely on vegetative reproduction, as *C. amara* did, which means that the selection pressure on faithful meiosis is expected to be fully intact. This system, the *Cochlearia* genus, is also more distantly related to *A. arenosa* and harbored at least 5 polyploidy events in the last 300,000 years.[19] The *Cochlearia* genus exhibits diploid, tetraploid, and higher cytotypes (Figure 1A),[19–22] with the very successful autotetraploid cytotype[19] similar in age to *A. arenosa*.[23,24] *Cochlearia* is found across Europe, from Spain to the Arctic, in a wide range of habitats, including freshwater springs, coastal cliffs, sand dunes, salt marshes, metal-contaminated sites, and roadside grit (Figure 1A).[19,25–35] A broad (but not exclusive) general habitat differentiation is evident by ploidy, with diploids most often found in upland freshwater springs; autotetraploids broadly on coasts, often directly adjacent to seawater or continuously submerged; and higher ploidies in extreme salt marsh conditions or salted roadways.[28,36]

To infer the genes and processes under selection in the young successful autopolyploid *Cochlearia* species and then test for convergence with those found in *A. arenosa* and *C. amara*, we first assess *Cochlearia* demography by individually resequencing 113 plants from 33 diploid, autotetraploid, hexaploid, and outgroup populations from across its range. We then focus our analysis on closely related diploids and autotetraploids in the UK and assess meiotic behavior and stress resilience phenotypes in the autotetraploids vs. diploids. Next, we scan for selective sweeps associated with autopolyploid establishment and dissect candidate targets of adaptive evolution using functional protein modeling and identification of orthologous-derived sites from functional studies. Our results show convergence at the process level in each of these recent autopolyploid establishment events in three genera separated by ~40 million years. This indicates that similar adaptive processes likely establish these young polyploids but that specific genes recruited are far less constrained. Surprisingly, we also find very strong signals of autopolyploid adaptation in several kinetochore components in autotetraploid *C. officinalis*, pointing to a novel mechanism of adaptation to autopolyploid meiosis and mitosis.

Figure 1. Ploidy variation, genome assembly, sampling, and genetic structure

(A) *Cochlearia* species in this study. Metaphase chromosomes counterstained with DAPI. Scale bars, 10 μm.

(B) Hi-C contact map and fluorescent *in situ* hybridization. Metaphase chromosomes counterstained with DAPI (blue) and hybridized with 102 bp satellite (pink) and telomeric (green) probes. Scale bar, 10 μm.

(C) Chromosome-scale assembly of diploid *C. excelsa* genome.

(D) *Cochlearia* populations sequenced (Data S2).

(E) Principal-component analysis of diploids (blue) and autotetraploids (orange). Principal component 1 (PC1) explains 21% of the variation and discriminates populations based on ploidy. PC2 explains only 9% of the variation and separates Norwegian tetraploids from UK tetraploids. Axes are scaled to contribution of each of the first PCs to the overall variation. NO, Norway; UK, United Kingdom; ES, Spain; SK, Slovakia; DE, Germany.

(F) fastSTRUCTURE[37] analysis of all *Cochlearia* individuals.

The same color legend applies to (A) and (D)–(F): blue indicates diploids; orange indicates tetraploids; green indicates hexaploids.

See also Figures S1 and S2 and Tables S1 and S2.

RESULTS

Chromosome-level *Cochlearia excelsa* assembly and annotation

First, to serve as a reference for our demographic analysis and selection scans, we built a chromosome-level genome assembly of one diploid *Cochlearia excelsa* individual (Styria, Gurktaler Alpen, Austria). We chose *C. excelsa* because it is an early-diverging diploid and, conveniently, also a rare, primarily selfing *Cochlearia* species. This resulted in a contiguous primary assembly (contig N50 = 15 Mb; Figure 1B), generated from Oxford Nanopore PromethION data (read N50 = 27 kb). The primary assembly was performed with Flye 2.9[38] and NECAT.[39] The assembled contigs were then scaffolded to chromosome-scale using Hi-C (Figure 1B), and a final cleanup was performed with Blobtools[40] (Figure S1A). Hi-C-guided chromosome arm orientations were confirmed with fluorescence *in situ* hybridization (FISH) and *in silico* mapping of telomeric and centromeric repeats (Figure 1B; Figures S1B and S1C). The assembly showed high completeness (97.3%) in a kmer-based analysis using independent read kmer assessment.[41] The six primary scaffolds corresponded to the six *C. excelsa* chromosomes with a scaffold N50 of 37 Mb and an overall genome size of 310 Mb (Figures 1B and 1C; Table S1), matching our estimated haploid genome size of 302 Mb in GenomeScope[42] (Figure S2A). Concordance between our FISH and *in silico* mapping of the probes over our continuous large scaffolds indicate that our assembly is a telomere-to-telomere representation of the *C. excelsa* genome (Figures S1B and S1C). Gene space representation was excellent, with 98% complete Brassicales BUSCOs[43] (Table S1) using Compleasm.[44] Addition of the small scaffold debris represented by scaffolds 7–115 gave 0 additional BUSCOs. These small scaffolds were comprised of 83% masked repeats with overwhelming contact associations with the centromeres in the HiC contact map (Figure 1B), indicating that these are predominantly uncollapsed repeats with little gene content (Table S2). Finally, we performed an annotation incorporating RNA sequencing data from the reference line, protein homology information, and *ab initio* modeling with BRAKER2.[45] This yielded 46,972 gene models.

Population sampling and ploidy confirmation

We set out to determine the optimal population contrasts to detect autopolyploidy-specific signatures of selection. To this end, we performed broad sampling of populations across the reported range of *Cochlearia* species throughout Europe[19,22,27–30,32,33,35] and then conducted flow cytometry-, cytology-, and kmer-based surveys of genome size and ploidy variation (Figure 1A; Data S1; Figure S2). Flow measurements were normalized against the diploid population with the most stable within-population genome size estimates, WOL (Data S1). We focus our demographic analysis on the three vastly most abundant ploidies (Figure 1A): diploids = *Cochlearia pyrenaica*, tetraploids = *Cochlearia officinalis*, and hexaploids = *Cochlearia danica*.

Establishment of *C. officinalis* as autotetraploid

While we include outgroups and sister species *Ionopsidium* and hexaploid *C. danica* in the genetic structure analysis, our focus in this study in the selection scans below is on adaptation to autopolyploidy. Thus, it was essential to confirm whether our abundant focal tetraploid, *C. officinalis*, arose from the combination of two genomes of the same (autopolyploid) or different (allopolyploid) species. Using deep (>120×) PCR-free Illumina sequencing of *C. officinalis*, we establish autopolyploidy with a kmer-based analyses and inspection of allele states (Figures S2C and S2D). This confirms the suitability of *C. officinalis* for comparisons of diploidy vs. autotetraploidy without the confounding factor of hybridization that would accompany allopolyploidy.

Population sequencing and genetic structure analysis

To focus our sampling on adaptation to autopolyploidy, we sampled primarily across the diploid-autopolyploid contrast but also with outgroups to provide a robust genetic structure analysis (113 individuals: 39 diploid, 67 tetraploid, 3 hexaploid, and 4 outgroup). These originated from 33 populations (10 diploid, 18 tetraploid, 2 hexaploid, and 3 outgroup). We sequenced all individuals by Illumina P150 (average per-individual depth = 17×; minimum = 4×; Figure 1D; Data S2). Read mapping to our diploid reference was efficient in all ploidies (average read mapping percentage per ploidy: diploids = 96%, autotetraploids = 93%, and hexaploids = 94%; Data S2), reflecting the shallow divergence between *Cochlearia* species.[19] We used a well-established[18,23,46–48] polyploid-specific pipeline to call variants and filter data with appropriate ploidy flags for each individual and perform demographic analyses. The final dataset consisted of 18,307,309 SNPs, on average one variant every 17 bp. This VCF was then passed through polyploid-aware analyses, following established best practices (STAR Methods; theory elaborated upon in Bohutínská et al.[46]).

To assess genetic structure, we first performed fastSTRUCTURE[37] (Figure 1F) on our 109 *Cochlearia* individuals, excluding the outgroup sister genus *Ionopsidium*. We used 23,733 unlinked (linkage disequilibrium-pruned minimum = 5 kb and r^2 = 0.2) and 4-fold degenerate (proxies of neutral sites) SNPs. We included sites only with a maximum 20% missing data and minimum minor allele frequency = 0.02. K = 3 maximized the marginal likelihood and grouped samples neatly by ploidy. Focusing on diploids vs. autotetraploids, principal-component analysis confirmed that ploidy dominates over geography (PC1 [ploidy] = 21% of variance explained; PC2 [UK vs. Norwegian tetraploids] = 9% of variance explained; Figure 1E). Interestingly, a single diploid population, the *C. aestuaria* population VEG of Northern Spain, clusters with the autotetraploids, suggesting a single origin from this diploid. We reconfirmed diploidy and homozygosity in this sample (Figures S2E and S2F).

Meiotic behavior in diploid vs. autopolyploid *Cochlearia*

Young autopolyploids tend to form tetravalents, associated eventually with aneuploidy.[6] We therefore investigated the meiotic behavior of *C. officinalis* to estimate whether they are in fact adapted to their autotetraploid state. Similar to *A. arenosa* autotetraploids,[12] we found a significant per-bivalent reduction in class I mature crossovers, evidenced by HEI10 foci (diploids = 2.28, tetraploids = 2.08; $p < 0.00001$; Mann-Whitney; Figures 2A,

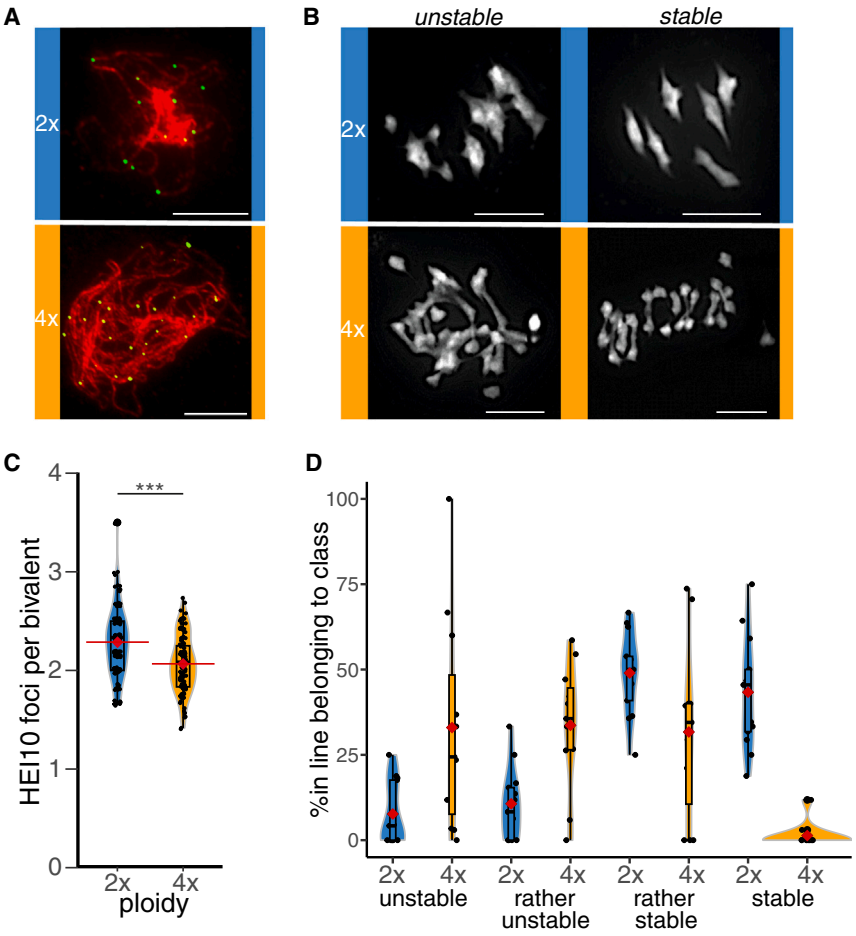

Figure 2. Meiotic behavior in autotetraploids relative to diploids

(A and C) Quantification of mature crossovers by HEI10 staining (green) on pachytene chromosomes stained by ZYP1 (red) (A), showing a significant (***$p < 0.00001$; Mann-Whitney) downregulation of crossovers in autotetraploids (C); see Figure S3 for split-channel images.

(B and D) Metaphase I chromosome spreads (B) and stability quantification by visualization of multivalents (D) showing higher proportions of multivalents in tetraploids (orange) relative to diploids (blue). Blue indicates diploids; orange indicates tetraploids. Scale bars, 10 μm.

See also Figure S3 and Table S3.

2C, and S3). Despite the reduction in the number of class I crossovers per chromosome, we still observed greater overall meiotic instability in the tetraploid compared with the diploid (Figures 2B and 2D), with dramatic variation in multivalent production both within and between populations (Table S3). By assessing the number of multivalents (STAR Methods), diploid lines were more frequently estimated to be "highly stable," and more autotetraploid lines had high variability, suggesting segregation for stabilizing factors (Figure 2D; Table S3).

Increased drought tolerance in autopolyploid *C. officinalis*

A second common phenotype evidencing adaptation to the polyploid state is increased drought or salinity stress resilience. A direct link between genome doubling and salinity tolerance was established in *Arabidopsis thaliana*, where first-generation neoautopolyploids (otherwise isogenic with diploid siblings) show elevated salinity tolerance and intracellular potassium.[49] These results motivate this question additionally due to the prevalent increased dehydration stress tolerance observed in higher ploidies relative to lower ploidies[5] and the accompanying cytoplasmic ionomic changes that are thought to mediate increased dehydration stress, in particular high potassium.[49,50] In the case of *Cochlearia*, accessions exhibit a broadly (but not exclusively) disjunct geographic distribution by ploidy, with diploids ($2n = 12$) deeply inland and autotetraploids inhabiting coastal regions of high salinity, including full seawater submergence (Figure S4). We therefore tested for ploidy-related differences in salinity tolerance and dehydration stress tolerance. Interestingly, in terms of overall plant survival, we found extreme salinity tolerance in all ecotypes tested, with even diploids tolerating up to 600 mM NaCl (salinity level of seawater), along with all higher ploidies (Table S4). Tetraploids showed signals of increased drought tolerance, with both elevated stomatal conductance and net photosynthetic rates under drought, relative to diploids (Figures 3A and 3B; Tables S4–S7). This suggests an adaptive benefit specific to higher ploidies in response to drought.

Selective sweeps associated with successful autopolyploid establishment

To identify candidate genes and processes involved in stabilizing autotetraploid *C. officinalis*, we next focused on the 18 geographically proximal populations from the UK (44 autotetraploid individuals and 29 diploid individuals; no allohexaploids were included in the below analyses). Concentrating the selection scan on UK diploids and autotetraploids minimizes the effects of genetic structure. To guide our window size choice, we calculated pairwise linkage decay, which was rapid in both ploidies, with near-complete loss of genotypic correlations within 2 kb to low background levels (Figure 4A). We thus calculated in 1 kb windows a battery of differentiation metrics (Dxy,[51] Rho,[52] Hudson's F_{ST},[53] Nei's F_{ST},[54] Weir-Cockerham's F_{ST},[55] and groupwise allele frequency difference [AFD]) genome wide (minimum = 15; mean = 101 SNPs per window). After filtering, these scans overlapped 86% of genes (40,245 of 46,972).

To determine which metric most reliably identified genomic regions that exhibit localized peaks in AFD indicative of specific sweeps upon autopolyploid establishment, we performed an inspection of all AFD plots in all outlier tails (STAR Methods). From

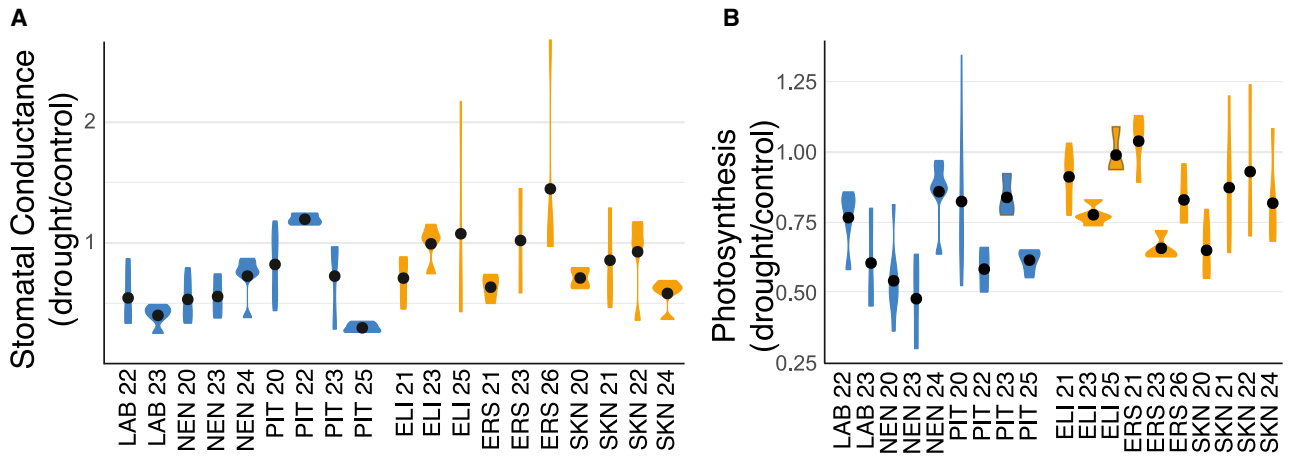

Figure 3. Improved drought response in autotetraploid *C. officinalis*

(A and B) Increased stomatal conductance (A) and photosynthetic (B) rates under dehydration stress in tetraploids. Plots show median and variation of drought-stressed plants in comparison to well-watered plants. Sign differences between diploids and tetraploids as seen in one-way ANOVA, post hoc Tukey (Table S7). Blue indicates diploids; orange indicates tetraploids.

See also Tables S4–S7.

this, we identified Hudson's F_{ST} as most reliably identifying localized AFD peaks (and not, e.g., low diversity[51]). This formulation of F_{ST} brings the added benefit of robustness for unequal sample sizes and the presence of rare variants[56] and direct comparisons to the *C. amara* study, which used this same metric. We therefore extracted windows in the top 1% of this distribution as candidate outliers, consisting of 1,823 1kb windows, overlapping 753 predicted genes for which we could obtain functional descriptions primarily from orthology (or, lacking this, close homology) to *A. thaliana* (Data S3). We focus on the most extreme 25 of these (right of the dashed line in Figure 4B; Table 1), which we confirm exhibit elevated Dxy values (outlier F_{ST} peak Dxy = 0.17; mean outside peak Dxy = 0.06; Mann-Whitney U test: $p < 2 \times 10^{-16}$; Figure 4C).

Complementing this approach, we also focused our 1% outlier list on gene-coding regions with a fineMAV approach.[76] Using Grantham scores to estimate the functional impact of each non-synonymous amino acid change encoded by a given SNP, this scales the severity of amino acid change by AFD between groups. Of 107,055 non-synonymous-encoding SNPs assigned a MAV score, the top 1% outliers from the empirical distribution were intersected with our F_{ST} outliers, yielding a protein-evolution-oriented list of 159 genes, harboring 290 MAV SNPs (bold in Data S3; 1% F_{ST} outliers with 10 or more 1% extreme MAV outliers are given in Table 1). By these approaches, we resolved gene-specific peaks of F_{ST} (Figure 5A) and candidate selective sweep alleles in our top 25 genome-wide outliers (Figures 5B–5G).

Finally, because ecotype preference and ploidy correlate within our dataset, we performed an additional selection scan designed to fully isolate the effect of ploidy. We excluded all coastal tetraploids, focusing only on inland tetraploids from salt-free environments (similar to the diploids) in an F_{ST} scan vs. diploids. Here, the same top outliers discussed above emerged again, with good concordance between the 1% outlier lists (outlier plots in Figure S5, mirroring Figures 5B–5G). Indeed, of the top 25 F_{ST} outliers in Table 1, 18 were present in both 1% outlier lists, including the DNA management and ion homeostasis genes discussed below (of the 7 remaining genes, 2 were absent from the second scan due to inadequate coverage in the smaller sample set).

DNA management, ion homeostasis, and cell stoichiometry processes under selection in autotetraploid *C. officinalis*

While we focus our discussion below on the top 25 genome-wide outliers, a broader, 1% F_{ST} list of 753 selective sweep candidates (Data S3) yields particularly informative Gene Ontology (GO) enrichments, with 181 significantly enriched categories (Data S4). Many of these categories can be grouped into three classes congruent with expected polyploid-associated changes[1,2,5–8,12]: (1) DNA management: 29 categories relate to DNA integration, cell division, meiotic chromosome segregation, mitosis, DNA repair, and recombination; 2) ion homeostasis: 26 categories relate to ion transport (principally extrusion), cation homeostasis, salt stress, and stomata; and (3) cell stoichiometry: 7 categories relate to global gene expression, cell wall, and biosynthesis, pointing to both global gene expression and nucleotypic[6] changes in polyploids.

Kinetochore evolution upon WGD

Genome wide, by far the strongest selection signature is directly over the coding region of the *CENTROMERE PROTEIN E* ortholog (*CENP-E*; Figures 5A and 5B).[77] This gene overlaps the 5 top F_{ST} outlier windows (mean F_{ST} = 0.88) and includes 37 of the 39 genome-wide fixed differences between ploidies. An essential kinetochore protein, *CENP-E* moves mono-oriented chromosomes to the spindle equator, mediating congression.[57,64,78] Strikingly, tetraploid cancers are far more susceptible to CENP-E inhibitors than diploids.[58–60,79,80]

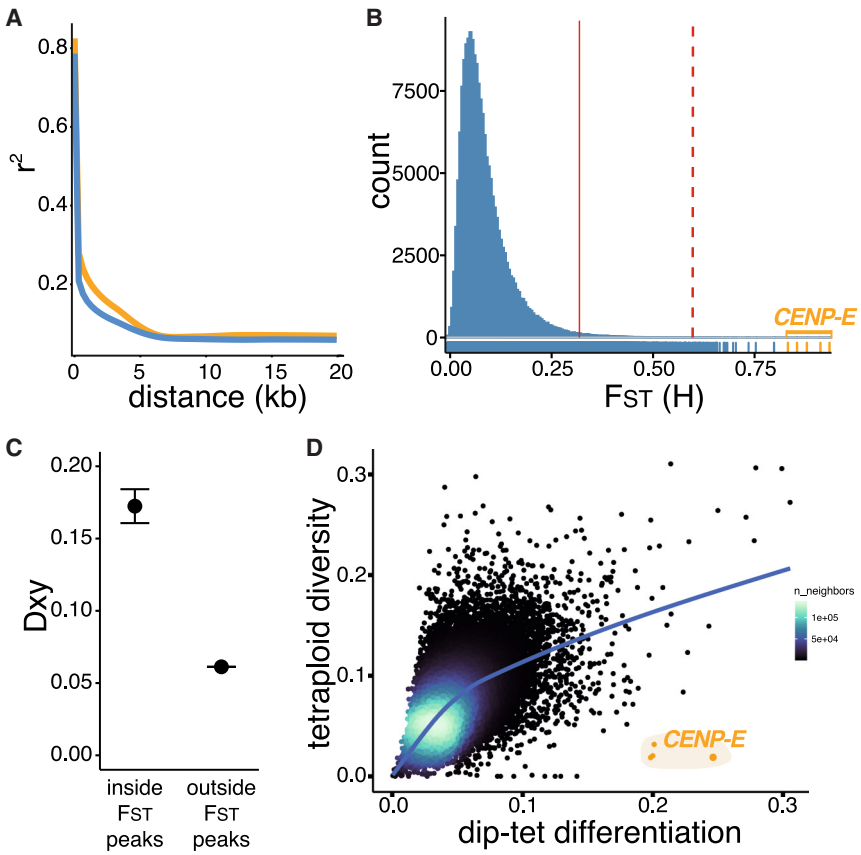

Figure 4. Rapid linkage decay and empirical outlier analysis

(A) Immediate decay of genotypic correlations (r^2) observed in both diploid (blue) and tetraploid (orange) *Cochlearia*.

(B) Distribution of genome-wide F_{ST} values for 182,327 1 kb windows. Dashed red line gives extreme stringency F_{ST} cutoff of the top 25 genome-wide outlier genes; solid red line gives the 1% cutoff; windows inside the *CENP-E* gene-coding region are highlighted in orange.

(C) Dxy values are significantly elevated inside F_{ST} peaks (Mann-Whitney U test: $p < 2 \times 10^{-16}$).

(D) *CENP-E*, the #1 genome-wide F_{ST} outlier, also exhibits greatly excess differentiation for its level of diversity in the tetraploids, a classical signal of selective sweep.

The *Cochlearia* CENP-E coding region contains 26 SNPs (synonymous or non-synonymous) that are highly differentiated between diploids and tetraploids (>50% AFD). Six of these are unique to *Cochlearia* tetraploids at highly conserved sites across angiosperms (Figure 6A). None are in characterized conserved functional regions of the kinase domain,[81] meaning motor activity is likely intact. Most of the tetraploid-specific changes are in the coiled-coil regions, which, in animals, are important for the regulation of cell division via phosphorylation and protein-protein interactions.[57] For example, point mutations in the coiled coils are associated with human disease (e.g., microcephaly[82,83]). In humans and *Xenopus*, these regions are known to be extensively phosphorylated during the cell cycle and may be involved in the autoinhibition of CENP-E.[84–87] Indeed, we see four tetraploid-specific changes that may affect regulation via the loss of phosphorylation (S717A, S821A, S1059L, and S1169Δ). Three additional changes toward the C terminus are in a cargo (chromosomes) binding region. Four of the tetraploid-specific changes show remarkable conservation across plants, being otherwise absolutely conserved across CENP-E-like kinesins (Figure 6A; A607G, Q613D, R899Q, and Q1024E). Taken together, these data suggest the changed regulation of CENP-E. This is consistent with functional evidence from *A. thaliana* showing that *CENP-E* mutations extend the cell cycle.[87]

Our top outlier list (Table 1) contains two additional orthologs of *A. thaliana* kinetochore components: *CENP-C*, an essential kinetochore component in both mitosis and meiosis needed for centromere identity in plants, yeast, *Drosophila*, and humans[65,66,88] (Figure 5C), and *INNER CENP* (*INCENP*), which controls mitotic and meiotic chromosome segregation and cytokinesis in plants, yeast, and animals.[75,89] At mitosis and meiosis, *INCENP* localizes to kinetochores and, later, the phragmoplast as the main subunit of the chromosome passenger complex.[74] Both INCENP and CENP-C contain 1% outlier-MAV SNPs, with *INCENP* harboring a remarkable 15 MAV outlier SNPs, the greatest number of any gene in the genome. In order to investigate whether other kinetochore-related genes might be exhibiting high, but not extreme, levels of selective sweep, we also performed explicit searches for selection signal in an exhaustive list of 131 kinetochore-related *Cochlearia* genes based on homology to annotated loci in model systems (Data S5, kinetochore-related genes). Among these, we found no compelling selection signal, revealing no further candidates. This underscores that the signal we discuss at CENP-C, CENP-E, INCENP, and related genes (Table 1; Data S3) is specific to those genes and the processes they mediate, not to wider related processes.

Evolution of DNA repair and transcription

Several of the top signals of selective sweeps are in DNA repair-related genes, for example, *CONDENSIN-II COMPLEX SUBUNIT H2/HYPERSENSITIVITY TO EXCESS BORON 2* (Figure 5D), which functions directly in double-strand break (DSB) repair[68,90] and chromatin management in plants, mouse, and *Drosophila*.[69,91] *Condensin II* is required for proper DNA DSB repair by homologous recombination (HR) repair in *A. thaliana* and humans[68,70] and has been implicated in the association and dissociation of centromeres.[91] We find in our 1% F_{ST} outliers an outlier also at a homolog of *DAYSLEEPER*, an essential domesticated transposase.[92] *DAYSLEEPER* binds the Kubox1 motif upstream of the DNA repair gene *Ku70* to regulate non-homologous end joining DSB repair, the only alternative to HR.[93,94]

Table 1. Top selective sweep candidates in autopolyploid *C. officinalis*

F_{ST} rank	*Cochlearia* ID	*thaliana* ID	Name	Description
1[a]	g7445	AT3G10180	CENP-E	CENTROMERE PROTEIN E: kinetochore protein that moves mono-oriented chromosomes to the spindle equator[57]; cooperates with chromokinesins and dynein to mediate chromosome congression; activity is regulated by post-translational modifications, protein interactions, and autoinhibition; tetraploid cancers are far more susceptible to CENP-E inhibitors than diploids[58,59,60]
2	g31016	AT1G06670	NIH	NUCLEAR DEIH-BOX HELICASE: binds DNA without clear specificity[61]
3	g7446	AT3G10070	TAF12	TATA-ASSOCIATED II 58: controls stress-responsive root growth[62]
4	g40185	AT2G26690	NPF6.2	NITRATE TRANSPORTER 6.2: mediates drought stress response[63]
5	g25338	AT4G00060	MEE44	MATERNAL EFFECT EMBRO ARREST 44: part of the RNA TRAMP complex
6	g49945	AT1G15660	CENP-C	CENTROMERE PROTEIN C: Kinetochore protein that is critical for centromere identity in both mitosis and meiosis. Loss of CENP-C results in aneuploidy and cell death.[64] Necessary in mitotic cells for kinetochore assembly centromere establishment. Mutants also fail to retain centromeric SC in late pachytene.[65,66]
7	g25334	AT1G05940	CAT9	CATIONIC AMINO ACID TRANSPORTER 9
8	g25335	AT4G00026	SD3	SEGREGATION DISTORTION 3: mutants have lower ploidy[67]
9	g6996	AT3G16730	CAP-H2/HEB2	CONDENSIN-II COMPLEX SUBUNIT H2: functions in DSB repair and arranges interphase chromatin[68,69]; plays a role in alleviating DNA damage and genome integrity in *A. thaliana*[68]; condensin II-depleted human cells have a defect in homologous recombination-mediated repair[70]
10	g24649	AT5G40595	–	unknown protein
11	g24648	AT4G02000	–	Ta11-like non-LTR retrotransposon
12	g33330	AT1G54310	–	S-adenosyl-L-methionine-dependent methyltransferases superfamily protein
13	g40302	AT4G10310	HKT1	HIGH-AFFINITY K + TRANSPORTER 1: sodium transporter; mediates salinity tolerance in wild *A. thaliana* populations[71]; under selection post-WGD in *A. arenosa*[12]
14	g33311	AT5G61390	NEN2	NAC45/86-DEPENDENT EXONUCLEASE-DOMAIN PROTEIN 2
15	g10739	AT2G01980	SOS1	SALT OVERLY SENSITIVE 1: plasma membrane-localized Na+/H+ antiporter; extrudes Na+ from cells; is essential for salt and stress tolerance
16	g46402	AT1G77990	SULTR2	SULFATE TRANSPORTER 2; 2: a low-affinity sulfate transporter
17	g4631	AT5G19270	–	reverse transcriptase-like protein
18	g4632	AT2G07200	–	cysteine proteinases superfamily protein

(*Continued on next page*)

Table 1. *Continued*

F_{ST} rank	*Cochlearia* ID	*thaliana* ID	Name	Description
19	g25121	AT5G35970	–	P loop containing nucleoside triphosphate hydrolase superfamily protein
20	g45503	AT5G08620	STRS2	STRESS RESPONSE SUPPRESSOR 2: a DEA(D/H)-box helicase involved in drought, salt, and cold stress responses
21	g25112	AT5G35980	YAK1	YAK1-related: controls cell cycle and regulates drought tolerance[72,73]
22	g40349	AT4G11110	SPA2	SPA1-related 2: convergent with WGD adaptation in *A. arenosa*[12]
23	g54387	AT3G01420	DOX1	an alpha-dioxygenase involved in protection against oxidative stress
24	g25300	AT5G34940	GUS3	GLUCURONIDASE 3
25	g45090	AT1G65320	CBSX6	cystathionine beta-synthase family protein
15 MAV	g39361	AT5G55820	INCEP/WYRD	INNER CENTROMERE PROTEIN: the largest subunit of the chromosome passenger complex (CPC) and directly binds to all other subunits in animals and yeast[74]; the CPC ensures that all kinetochores are attached to microtubules emanating from opposing poles; INCENP is necessary for normal mitotic divisions[75]; at mitosis and meiosis localizes to kinetochores and, later, the phragmoplast[74]
12 MAV	g25323	AT4G29090	–	ribonuclease H-like superfamily protein
11 MAV	g23778	AT4G25290	–	DNA photolyase
11 MAV	g54385	AT1G56145	CORK1	an LRR receptor kinase required for cello oligomer-induced responses
10 MAV	g33400	AT1G50240	FU	FUSED: an ARM repeat domain-containing protein kinase involved in male meiosis; tightly localized to nascent phragmoplast and with the expanding phragmoplast ring

Top 25 of 40,245 genes assessed, with 5 additional genes (bottom) with 10 or more MAV SNPs and in the top 1% F_{ST} tail. Genome-wide F_{ST} rank is shown in column 1.
[a]Contains 37/39 whole-genome fixed differences between diploids and tetraploids and is also the only gene with three of the top 25 Dxy windows.

In a young polyploid, the total DNA content doubles, but the protein content and cell size do not scale accordingly,[8] so we predicted that the control of global gene expression, like meiosis, should undergo adaptive evolution post-WGD. Here, we see signals of this, with a suite of DNA or RNA polymerase-associated genes among our selective sweep outliers. In our 1% F_{ST} outliers, this includes *NRPB9*, an RNA polymerase subunit that is implicated in transcription initiation, processivity, fidelity, proofreading, and DNA repair,[95–99] as well as the ortholog of *MED13*, of the mediator complex, which is essential for the production of nearly all cellular transcripts[100] (Data S3).

Evolution of ion homeostasis, transport, and stress signaling

The ionomic equilibrium of the cell is immediately disrupted at WGD[49]; in particular, K^+ concentrations are increased instantly, consistent with increases in salinity tolerance in synthetic *A. thaliana* autotetraploids.[49] In our young tetraploids, among the top selective sweeps are ion channels that function explicitly to remove K^+, Na^+, and other cations from the cell. At F_{ST} rank 13 genome wide, we see the ortholog of *HIGH-AFFINITY K^+ TRANSPORTER*[71,101] (*HKT1*; Figures 5G and 6B), and at rank 15, we see *SALT OVERLY SENSITIVE 1* (*SOS1*), a membrane Na^+/H^+ transporter that removes excessive Na^+ from the cell and is central to salt tolerance[102,103] (Figure 5F).

Structural homology modeling confirms that the *Cochlearia HKT* under selection is class 1 from its selectivity filter residue configuration (S-G-G-G), indicating that it is likely Na^+ selective (and K^+ non-selective).[104] There is an L344V mutation in the tetraploid relative to the diploid; remarkably, this is the identical site and amino acid change that is associated with salt tolerance in rice OsHKT1; 5 (Figure 6B)[105,106]: functional confirmation in rice shows that the orthologous site substitution to valine in our tetraploid is associated with salt tolerance (including faster Na^+ transport), while the diploid leucine is associated with salt sensitivity (including slower Na^+ transport).[105] Given that the tetraploids live overwhelmingly in coastal regions where they are exposed to extreme Na levels, while the diploid lives in low-Na freshwater streams, this makes biological sense. While the close proximity of L344 alone is likely enough to disrupt pore rigidity via

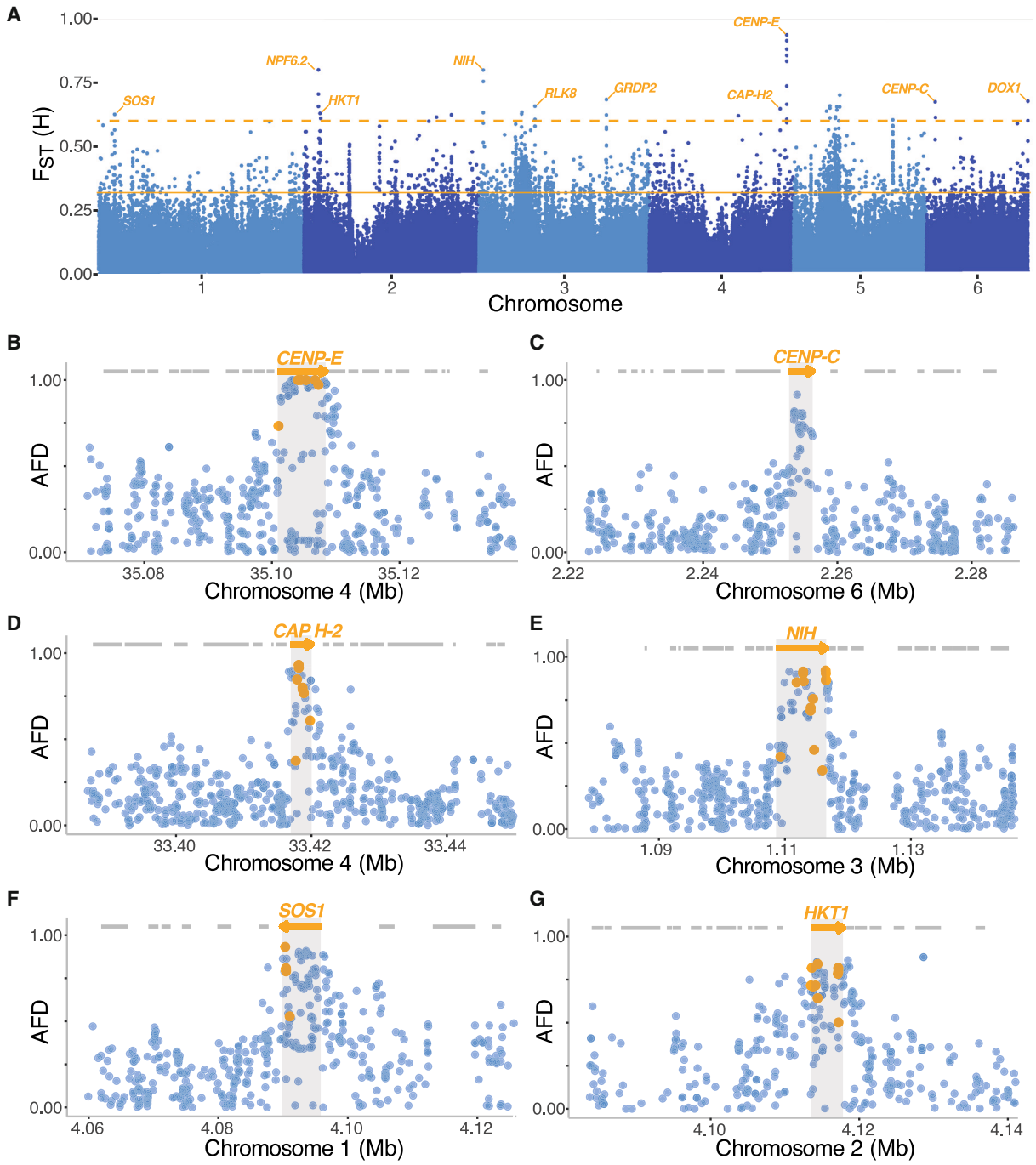

Figure 5. Selective sweep signatures of DNA management and ion homeostasis alleles

(A) Ploidy-specific differentiation across the *Cochlearia* genome. The dashed orange line gives the extreme stringency F_{ST} cutoff of the top 25 outlier genes; the solid line gives a 1% F_{ST} cutoff.

(B–G) Examples of 6 outlier genes. (B)–(E) represent kinetochore or DNA management. (F and G) Ion homeostasis functional categories. The x axis gives genome position. The y axis gives AFD values at single SNPs (dots) between diploid and tetraploid *Cochlearia*. Orange arrows indicate genes overlapping the top F_{ST} outlier windows; gray lines indicate neighboring genes. Orange dots indicate MAV outliers.

See Figures S5 and S6.

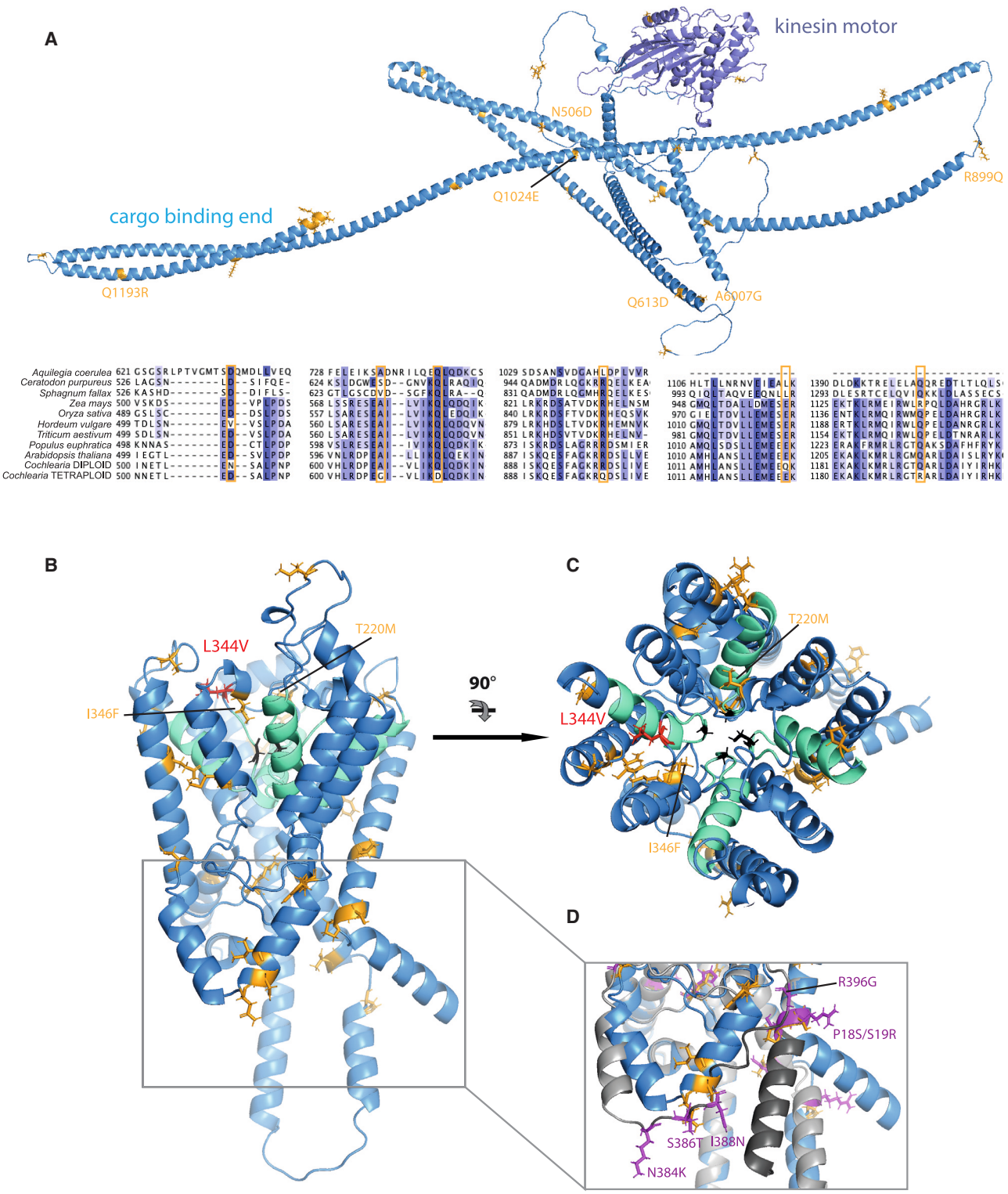

Figure 6. Tetraploid-derived protein structure changes in CENP-E and HKT1

(A) Kinetochore subunit CENP-E structural prediction and diversity. Structure: diploid structure (blue), consensus (>50% allele frequency)-derived polymorphisms in tetraploids (orange), and kinesin motor domain (slate). Alignment: color by percentage identity; consensus mutations at highly conserved sites (orange boxes).

(legend continued on next page)

its larger side chain relative to V, in *Cochlearia* HKT1, we also see T220M (a highly conserved residue) and I346F mutations, which are even closer to the P1-4 pore domains that hold S-G2-G3-G4 together to create the selectivity control. These mutations all introduce large side chains that likely affect structural dynamics at the P1-4 pore.[105,106] In addition, the mutations F326I, R200P L180F, Q303H, and M360I are all in (R200P and F326I), or in contact with, the four alpha helices that stabilize the SGGG selectivity filter. While this may seem an excessive quantity of mutations, suggesting gene inactivation, all the sites except M360I, T220M, and L344V are loosely conserved, suggesting flexibility in these regions.

There are also mutations on the cytosolic side of the protein, where a few poorly conserved residues appear to induce small structural changes (Figure 6D). This includes a cluster of changed residues (I388N, S386T, N384K, R396G), which are predicted to break up an alpha helicase in the tetraploid, and P18S and S19R, which appear to induce a break in the first alpha helicase of the protein. To our knowledge, this domain is not functionally characterized, though given this positioning, it could represent a change in signaling or regulation.

Congruent with its conserved central role in ion homeostasis, *SOS1* is highly conserved, and tetraploid-specific changes are not near transport binding sites (nucleotide or ion), nor dimerization domains. Instead, a tight cluster of 3 mutations marks the boundary between the β-sheet-rich cytoplasmic domain and the C-terminal autoinhibition (CTA) domain, which contains a further 3 mutations (K1014E, T1075S, and R1101Q). The CTA is unstructured; however, it has been experimentally shown that just two point mutations can change the behavior of the channel, presumably by releasing autoinhibition, increasing Na^+ transport, and, therefore, increasing salt tolerance.[107] Notably, this includes one T1075S substitution: S and T are two of the three amino acids that can be phosphorylated, and it has been shown that these two residues behave differently when phosphorylated, suggesting that the choice of S or T may have evolutionary consequences.[108]

Ion homeostasis shifts should be associated with changes in responses to salt, osmotic, and cold stress, as all these stressors have a common osmotic basis. Such a link between immediate ionomic changes in the polyploid cell may be a key functional basis for the observed ecotypic differentiation of young polyploids, especially as observed in arctic and alpine conditions. We accordingly see in our top outliers categories of relevant genes, e.g., *DEAD-BOX RNA HELICASE 25* (*STRS2*), identified in *A. thaliana* as a repressor of stress signaling for salt, osmotic, and cold stress.[109,110] This gene also controls freezing tolerance,[111] relevant to the cold-loving arctic and alpine history of *Cochlearia*.[19]

Functional relevance of ion homeostasis shifts in diploids vs. autotetraploids

To assess whether these sweeps were better associated with ecotype differentiation between ploidies rather than adaptation to autopolyploidy, we performed a salt tolerance experiment on diploid and autotetraploid plants. Interestingly, given their divergent ecotype preferences (Figure S4), with tetraploids found in more saline conditions, we found that the diploid *Cochlearia* are in fact more salt tolerant than the tetraploids ($p = 2.178 \times 10^{-05}$; see STAR Methods and Table S4.). This finding also contrasts with observations of increased salinity tolerance in neotetraploid *A. thaliana*.[49] Again, however, this may be a signal of preadaptation to osmotic challenge (common to freezing, salinity, and dehydration) across the halophyte *Cochlearia*.[112]

Gene-level convergence

To test for convergence at the ortholog level, we first determined orthogroups[113] between *Cochlearia*, *A. arenosa*, and *C. amara*. We then compared our top 1% F_{ST} candidate list for *Cochlearia* ($n = 753$; Data S3) with those published by the same empirical 1% F_{ST} outlier approach[18] in *A. arenosa* ($n = 452$; Data S6), and *C. amara* ($n = 229$; Data S7). For all cases, genes were considered orthologs if they were part of the same orthogroup. By this criterion, not a single ortholog was under selection in all three species (Figure S6A; Data S8). This approach depends on strict 3-way orthogroup assignment, so we then searched for convergence by assigning all genes in the outlier lists to the nearest *A. thaliana* homolog. By this "nearest homolog" criterion, only one gene was selected in all three WGDs: *DAYSLEEPER*, an essential domesticated transposase[92] with a role in regulating non-homologous end joining DSB repair (Figure S6B; Data S9).

Interestingly, by both homolog assignment methods, several of the *Cochlearia* WGD adaptation candidates were found to be present also in *A. arenosa*. *ASY3* (Figure S6D), functionally validated[14,17] to have a role in stabilizing autotetraploid meiosis in *A. arenosa*, is also in our 1% F_{ST} outlier list in *Cochlearia*.[14] We also see *CYCD5;1*, which is a quantitative trait locus for endoreduplication.[114] Additionally, the salinity and osmotic genes *HKT1* and *OST2* are in both top candidate lists (Data S8). All these genes are involved in processes that have been implicated in adaptation to WGD[1,2,5,6,8,12] and therefore stand as good candidates to mediate adaptation to salient challenges to nascent polyploids. We note that overlap between *Cochlearia* and both *A. arenosa* and *C. amara* candidates was greater than expected by chance (SuperExactTest[115] $p = 0.0024$ and $p = 0.0047$, respectively) but only marginally so for *C. amara* and *A. arenosa* (SuperExactTest $p = 0.014$).

Process-level convergence

We reasoned that there may be similarities in processes under selection between the three independent WGDs, despite modest gene-level convergence. To test this, we first compared our GO results with those published in *A. arenosa* and *C. amara*. The much greater signal of overlap (process-level convergence; Figure S6C) was found between *Cochlearia* and *A. arenosa*: of the 113 GO biological process terms significantly enriched in *Cochlearia*, 17 were among the 73 GO terms enriched in

(B–D) Ion channel HKT1: diploid structure (blue), mutation sites (orange; diploids, magenta: tetraploids), pore domains (teal). (C) HKT1 extracellular surface. Salinity tolerance-mediating change L344V in red and selectivity filter residues S/G1, G2, G3, and G4 (black). (D) Super-imposition of diploid (blue) and tetraploid (gray) intracellular domains. Structures that are predicted to have rotated are highlighted on the tetraploid structure (dark gray). Tetraploid consensus mutations (magenta).

A. arenosa (Data S4; $p = 0$ in permutation tests). These were high-level GO terms including representatives of ploidy-relevant categories, e.g., "cell division," "transmembrane transport," and "regulation of RNA metabolic processes."

Further evidence of functional association between outliers found in *Cochlearia* and those in *A. arenosa* is observed in protein interaction information from the STRING database, which provides an estimate of proteins' joint contributions to shared function.[116] Using comparable 1% F_{ST} outlier lists from the two species, we see many connections between these independent WGDs. Here, we see particularly large clusters (Figures S6E and S6F) in the center of the overall network (Figure S6G). In particular, the endopolyploidy gene[114] *CYCD5;1* and *DNA Pol V* (a shared outlier in both species) interact with many other outliers in each selection scan (Figure S6E). This analysis reveals, for example, that *DNA Pol V* occurs as a top candidate alongside either *NRPB9A* (in *A. arenosa*) or *NRPB9B* (in *Cochlearia*). These subunits are partly redundant interactors with *Pol II, -IV*, and *-V*, and the double mutant is fatal in *A. thaliana*.[97]

DISCUSSION

A rich literature cataloging phenotypic shifts upon ploidy increase tells us that each polyploidy event represents a unique evolutionary experiment.[1–3,5,6,8] However, common themes emerge, evidenced by fairly consistent changes in the cell. First, a multiplication of DNA content may complicate meiotic pairing, recombination, and segregation of the added genome copies, especially in autopolyploids.[117] A survey of 67 ploidy-variable species distilled the most common phenotypic alterations to include also cell size increases and elevated stress tolerance, especially to drought and salt.[5] Associated with these phenotypes are ion homeostasis shifts[49] and changes to stomatal function.[1,2,5,8] Underlying these phenotypes are cell-scaling changes that occur immediately upon WGD, usually including increased overall sizes and altered ratios of cell volume to surface area (tetraploid cell volume is measured at twice that of diploid progenitors, but the surface area is 1.6 times greater).[118] Accordingly, these changes impact relative stoichiometries of many cellular components.[5,8] Elemental concentrations can be distorted: for example, first-generation *A. thaliana* neoautopolyploids consistently exhibit increased potassium concentrations, which associate with increased dehydration stress tolerance.[49] Thus, we can expect nascent polyploids to have to retune their cellular physiology to their new reality.

We sought here to understand what shared evolutionary optimizations autopolyploids make in response to WGD-associated cellular shifts. In particular, we tested whether the focused signal of meiotic adaptation discovered in *A. arenosa*[12] is recapitulated in a similar autopolyploid system, *C. officinalis*. Instead of the suite of coevolving[119] meiotic crossover-controlling proteins found in *A arenosa*, we see the strongest evidence of selective sweep at kinetochore components *CENP-E*, *CENP-C*, *INCENP*, and *CAP-H2*, as well as well-studied ion homeostasis loci *HKT1* and *SOS1*. By far, the most extreme selective sweep signature covers the *CENP-E* gene-coding locus (Figure 5). *CENP-E* moves mono-oriented chromosomes to the spindle equator, mediating congression,[57,64,78] with a direct link to polyploidy in human cancers: strikingly, tetraploid cancers are far more susceptible to CENP-E inhibitors than diploids.[58–60,79,80] This, combined with our identification of the differentiation of other kinetochore components *CENP-C* and *INCENP*, points to mitotic and meiotic chromosome segregation[75,89] as the target of optimizations, in particular highlighting the phragmoplast.[74] Given previous observations of meiotic adaptation to WGD in *A. arenosa*, a connection to meiosis would be unsurprising; however, these loci are more generally engaged in mitotic cell division. Of course, mitosis must also be well orchestrated before meiosis would matter: mitotically unstable neotetraploids would most likely never engage in meiosis.

That said, there appears more in common between the meiosis solution found in *A. arenosa* and the one here evidenced in *C. officinalis*. In *A. arenosa*, a focused prophase I-oriented signal emerged primarily around synaptonemal complex (SC)-associated proteins mediating lower crossover rates in the autotetraploid.[12] Notably, *CENP-C* mutants fail to retain centromeric SCs, and *CENP-C* appears to function in synapsis, cohesion, and centromere clustering.[120] Thus, *CENP-C* may serve as a bridge between earlier prophase homolog synapsis and later metaphase kinetochore assembly.[65] In addition, other SC-related genes emerge: while not exhibiting the most dramatic signatures of selective sweep we see in the kinetochore components, a variety of other meiosis-related genes exhibit selection signal in *C. officinalis* (genome-wide top 1% F_{ST} outliers; Data S3). Most conspicuous among these is *ASY3* (Figure S6D). In *A. arenosa*, derived, polyploid-specific alleles of *ASY3* (along with *ASY1*) result in fewer multichromosome associations, which are less prone to deleterious outcomes.[17] However, dedicated searches for selection signals in the suite of meiosis genes under selection in *A. arenosa* revealed only ASY3 as a candidate under selection in *C. officinalis*. Interestingly, other meiosis-related genes show differentiation signals in *C. officinalis* that do not show any signal in *A. arenosa*, such as *ATM* (*ATAXIA TELANGIECTASIA MUTATED*), which controls meiotic DNA DSB formation and recombination and affects SC organization.[121] We also see the *PDS5* cohesion cofactor ortholog *RMI1* (*RECQ MEDIATED INSTABILITY 1*), which suppresses somatic crossovers and is essential for the resolution of meiotic recombination intermediates.[122] Notable also are *BRCA2-like B* (essential at meiosis and interacts with *Rad51*, *Dss1*, and *Dmc1*) and *SHUGOSHIN C* (protects meiotic centromere cohesion). Thus, there appears to be substantial parallelism between the obviously "SC-focused" adaptive response in *A. arenosa* and the evolutionary response to WGD in *C. officinalis*, although the signal in *C. officinalis* is less concentrated on interacting partners at the SC itself in favor of a broader array of DNA management and meiosis-related genes.

The relatively diffuse signal at meiosis genes is accompanied by a more focused signal at the kinetochore in *C. officinalis* and partnered with the suggestion of other, diverse evolutionary responses around DNA management and ion homeostasis. While most of these categories are represented in *A. arenosa*, no strong selection is evident on kinetochore proteins in *A. arenosa*. It is unclear why particular solutions are favored in one species relative to another. A degree of stochasticity depending on available standing variation can be expected, but

species histories likely play a role, offering preadaptations that may "nudge" an evolutionary trajectory down another path. For example, ion homeostasis, and especially genes involved in salinity tolerance, is well represented among the genes with the strongest signals of selection in *Cochlearia*, but in our functional comparisons between diploid and autopolyploid *Cochlearia*, we uncovered the surprising result that the diploid was at least as tolerant to extreme salt concentrations as the polyploid, although the diploid is found predominantly inland. A post-glacial and boreal spread of the diploid toward the UK may have brought salinity and cold tolerance along the way,[123] altering the genomic substrate upon which selection acted in response to polyploidy-associated ionomic challenge.

Finally, evidence of broader categories of DNA management and repair under selection at WGD also suggest a speculative hypothesis for the association long-observed between polyploidy and adaptation. We observed an array of DNA management and repair processes under selection in all three genera, especially *Cochlearia*. That these processes exhibit marked selective sweeps points to a selection pressure to adjust these processes early in autopolyploid establishment. We speculate that this may signal a temporarily increased susceptibility to DNA damage in the nascent autopolyploid, possibly due to an early suboptimal function of DNA repair—and certainly meiotic fidelity—during the process of adaptation to the novel polyploid state. This may effectively, therefore, result in a relative "mutator phenotype" in nascent autopolyploids. Such a mutator phenotype is plainly observed in polyploid metastatic human cancers, which not only exhibit SNP-level hypermutator phenotypes but also dramatic structural variation in malignant aneuploid swarms that are associated with cancer progression.[3] We suggest that a parallel to this may exist following other polyploidy events. Whether or not this hypothesis is further supported by future discoveries, the centrality of polyploidy to evolution, ecology, and agriculture, underscores the importance of understanding the processes mediating adaptation to—and perhaps also by—polyploidy in each of life's kingdoms.

Limitations of the study

From these findings alone, it is unresolved whether the primary function of the kinetochore-associated genes found under selection in the present study is mitotic or meiotic. Dedicated study of the effects of alternate (diploid or autotetraploid) candidate alleles on mitosis and meiosis is required to address this. Therefore, transgenics need to be developed in *Cochlearia*.

STAR★METHODS

Detailed methods are provided in the online version of this paper and include the following:

- KEY RESOURCES TABLE
- RESOURCE AVAILABILITY
  - Lead contacts
  - Materials availability
  - Data and code availability
- EXPERIMENTAL MODEL AND STUDY PARTICIPANT DETAILS
- METHOD DETAILS
  - Plant material
  - Ploidy determination by flow cytometry
  - HEI10 immunostaining
  - Chromosome number determination, meiotic stability estimation, and fluorescence *in situ* hybridization
  - Salinity tolerance experiments
  - Stomatal conductance assessment, net photosynthesis and drought tolerance experiments
  - Reference genome assembly and alignment
  - High molecular weight DNA isolation and Oxford Nanopore sequencing
  - Genome size estimation and computational ploidy inference
  - Data processing and assembly
  - Pseudomolecule construction by Hi-C, assembly cleanup, and polishing
  - Assembly annotation and RNA-seq
  - Population resequencing and analysis
- QUANTIFICATION AND STATISTICAL ANALYSIS
  - Quantification and statistical analysis

SUPPLEMENTAL INFORMATION

Supplemental information can be found online at https://doi.org/10.1016/j.celrep.2024.114576.

ACKNOWLEDGMENTS

We thank Kirsten Bomblies, Mary Bray, and Nigel Bray for assistance collecting plant material. We acknowledge wet-lab support from Anna Loreth. This work was supported by the European Union's Horizon 2020 research and innovation programme under the European Research Council grant agreement no. 679056 to L.Y. and under the Marie Skłodowska-Curie grant agreement no. 101022295 to T.H. We also acknowledge the UK Biotechnology and Biological Sciences Research Council grants (grant nos. BB/P013511/1 and BB/R017174/1) to L.Y. and a Leverhulme Trust award (no. RPG-2020-367) to L.Y. The results of this project LL2317 were obtained with the financial contribution of the Ministry of Education, Youth and Sports as part of the targeted support of the ERC CZ program. Computational resources were provided by the e-INFRA CZ project (ID: 90254), supported by the Ministry of Education, Youth and Sports of the Czech Republic. We thank local authorities for issuing permission to collect samples (Slovak Ministry for Environment, permission no. 062–219/18). The article is available in gold open access.

AUTHOR CONTRIBUTIONS

Conceptualization, L.Y. and S.M.B.; software, S.M.B.; resources, L.Y., S.M.B., M.A.K., P.M., M.A.L., and J.K.; investigation, S.M.B., S.B., S.D.D., T.M., C.M., L.C., M.Z., and S.F.; formal analysis, S.M.B., L.Y., T.H., S.D.D., C.M., T.C.M., T.M., E.M.W., S.B., S.F., M.A.K., and L.Y.; data curation, L.Y.; writing – original draft, L.Y. and S.M.B.; writing – review & editing, L.Y., S.M.B., F.K., and M.A.K.; visualization, L.Y.; supervision L.Y., J.D.H., and M.A.K.; project administration, L.Y. and M.A.K.; funding acquisition, L.Y., T.H., and M.A.K. All authors approved the final manuscript.

DECLARATION OF INTERESTS

The authors declare no competing interests.

Received: November 8, 2023
Revised: May 17, 2024
Accepted: July 18, 2024

REFERENCES

1. Yant, L., and Bomblies, K. (2015). Genome management and mismanagement–cell-level opportunities and challenges of whole-genome duplication. Genes Dev. *29*, 2405–2419. https://doi.org/10.1101/gad.271072.115.

2. Baduel, P., Bray, S., Vallejo-Marin, M., Kolář, F., and Yant, L. (2018). The "Polyploid Hop": Shifting Challenges and Opportunities Over the Evolutionary Lifespan of Genome Duplications. Front. Ecol. Evol. *6*, 117. https://doi.org/10.3389/fevo.2018.00117.

3. Van de Peer, Y., Mizrachi, E., and Marchal, K. (2017). The evolutionary significance of polyploidy. Nat. Rev. Genet. *18*, 411–424. https://doi.org/10.1038/nrg.2017.26.

4. Salman-Minkov, A., Sabath, N., and Mayrose, I. (2016). Whole-genome duplication as a key factor in crop domestication. Nat. Plants *2*, 16115. https://doi.org/10.1038/nplants.2016.115.

5. Bomblies, K. (2020). When everything changes at once: finding a new normal after genome duplication. Proc. Biol. Sci. *287*, 20202154. https://doi.org/10.1098/rspb.2020.2154.

6. Bomblies, K. (2023). Learning to tango with four (or more): the molecular basis of adaptation to polyploid meiosis. Plant Reprod. *36*, 107–124. https://doi.org/10.1007/s00497-022-00448-1.

7. Bomblies, K., Jones, G., Franklin, C., Zickler, D., and Kleckner, N. (2016). The challenge of evolving stable polyploidy: could an increase in "crossover interference distance" play a central role? Chromosoma *125*, 287–300.

8. Doyle, J.J., and Coate, J.E. (2019). Polyploidy, the Nucleotype, and Novelty: The Impact of Genome Doubling on the Biology of the Cell. Int. J. Plant Sci. *180*, 1–52. https://doi.org/10.1086/700636.

9. Van de Peer, Y., Ashman, T.L., Soltis, P.S., and Soltis, D.E. (2021). Polyploidy: an evolutionary and ecological force in stressful times. Plant Cell *33*, 11–26. https://doi.org/10.1093/plcell/koaa015.

10. Renny-Byfield, S., and Wendel, J.F. (2014). Doubling down on genomes: polyploidy and crop plants. Am. J. Bot. *101*, 1711–1725. https://doi.org/10.3732/ajb.1400119.

11. Pelé, A., Rousseau-Gueutin, M., and Chèvre, A.-M. (2018). Speciation Success of Polyploid Plants Closely Relates to the Regulation of Meiotic Recombination. Front. Plant Sci. *9*, 907. https://doi.org/10.3389/fpls.2018.00907.

12. Yant, L., Hollister, J.D., Wright, K.M., Arnold, B.J., Higgins, J.D., Franklin, F.C.H., and Bomblies, K. (2013). Meiotic adaptation to genome duplication in Arabidopsis arenosa. Curr. Biol. *23*, 2151–2156. https://doi.org/10.1016/j.cub.2013.08.059.

13. Hollister, J.D., Arnold, B.J., Svedin, E., Xue, K.S., Dilkes, B.P., and Bomblies, K. (2012). Genetic adaptation associated with genome-doubling in autotetraploid Arabidopsis arenosa. PLoS Genet. *8*, e1003093.

14. Seear, P.J., France, M.G., Gregory, C.L., Heavens, D., Schmickl, R., Yant, L., and Higgins, J.D. (2020). A novel allele of ASY3 is associated with greater meiotic stability in autotetraploid Arabidopsis lyrata. PLoS Genet. *16*, e1008900. https://doi.org/10.1371/journal.pgen.1008900.

15. Morgan, C., Knight, E., and Bomblies, K. (2022). The meiotic cohesin subunit REC8 contributes to multigenic adaptive evolution of autopolyploid meiosis in Arabidopsis arenosa. PLoS Genet. *18*, e1010304.

16. Morgan, C., White, M.A., Franklin, F.C.H., Zickler, D., Kleckner, N., and Bomblies, K. (2021). Evolution of crossover interference enables stable autopolyploidy by ensuring pairwise partner connections in Arabidopsis arenosa. Curr. Biol. *31*, 4713–4726.e4. https://doi.org/10.1016/j.cub.2021.08.028.

17. Morgan, C., Zhang, H., Henry, C.E., Franklin, F.C.H., and Bomblies, K. (2020). Derived alleles of two axis proteins affect meiotic traits in autotetraploid *Arabidopsis arenosa*. Proc. Natl. Acad. Sci. USA *117*, 8980–8988.

18. Bohutínská, M., Alston, M., Monnahan, P., Mandakova, T., Bray, S., Paajanen, P., Kolar, F., and Yant, L. (2021). Novelty and Convergence in Adaptation to Whole Genome Duplication. Mol. Biol. Evol. *38*, 3910–3924. https://doi.org/10.1093/molbev/msab096.

19. Wolf, E., Gaquerel, E., Scharmann, M., Yant, L., and Koch, M.A. (2021). Evolutionary footprints of a cold relic in a rapidly warming world. Elife *10*, e71572.

20. Gill JJB, M.H., and Fearn, G.M. (1978). Cytotaxonomic studies on the Cochlearia officinalis L. group from inland stations in Britain. Watsonia *12*, 15–21.

21. Gill, J.J.B. (1973). Cytogenetic studies in Cochlearia L.(Cruciferae). The origins of C. officinalis L. and C. micacea Marshall. Genetica *44*, 217–234.

22. Gill, J.J.B. (1971). Cytogenetic studies in Cochlearia L. The chromosomal homogeneity within both the 2 n= 12 diploids and the 2 n= 14 diploids and the cytogenetic relationship between the two chromosome levels. Ann. Bot. *35*, 947–956.

23. Marburger, S., Monnahan, P., Seear, P.J., Martin, S.H., Koch, J., Paajanen, P., Bohutínská, M., Higgins, J.D., Schmickl, R., and Yant, L. (2019). Interspecific introgression mediates adaptation to whole genome duplication. Nat. Commun. *10*, 5218. https://doi.org/10.1038/s41467-019-13159-5.

24. Arnold, B., Kim, S.-T., and Bomblies, K. (2015). Single geographic origin of a widespread autotetraploid Arabidopsis arenosa lineage followed by interploidy admixture. Mol. Biol. Evol. *32*, 1382–1395.

25. Fearn, G.M. (1977). A morphological and cytological investigation of Cochlearia populations on the Gower Peninsula, Glamorgan. New Phytol. *79*, 455–458.

26. Stace, C.A. (1975). Hybridization and the Flora of the British Isles. Botanical Society of the British Isles.

27. Koch, M. (2002). Genetic differentiation and speciation in prealpine Cochlearia: Allohexaploid Cochlearia bavarica Vogt (Brassicaceae) compared to its diploid ancestor Cochlearia pyrenaica DC. in Germany and Austria. Plant Systemat. Evol. *232*, 35–49.

28. Koch, M. (1996). Zur Ausbreitung des Dänischen Löffelkrautes (Cochlearia danica L.) als Küstensippe in das niedersächsische Binnenland. Florist. Rundbr. *30*, 20–23.

29. Koch, M. (1997). Kurznotiz zur südlichen Ausbreitung des Dänischen Löffelkrauts (Cochlearia danica L.) in Nordrhein-Westfalen. Florist. Rundbr. *30*, 136–138.

30. Koch, M., Dobeš, C., Bernhardt, K.-G., and Kochjarová, J. (2003). Cochlearia macrorrhiza (Brassicaceae): A bridging species between Cochlearia taxa from the Eastern Alps and the Carpathians? Plant Systemat. Evol. *242*, 137–147.

31. Koch, M., Hurka, H., and Mummenhoff, K. (1996). Chloroplast DNA restriction site variation and RAPD-analyses in Cochlearia (Brassicaceae): Biosystematics and speciation. Nord. J. Bot. *16*, 585–603.

32. Koch, M., Huthmann, M., and Hurka, H. (1998). Isozymes, speciation and evolution in the polyploid complex Cochlearia L.(Brassicaceae). Bot. Acta *111*, 411–425.

33. Koch, M., Mummenhoff, K., and Hurka, H. (1999). Molecular phylogenetics of Cochlearia (Brassicaceae) and allied genera based on nuclear ribosomal ITS DNA sequence analysis contradict traditional concepts of their evolutionary relationship. Plant Systemat. Evol. *216*, 207–230.

34. Koch, M.A. (2012). Mid-Miocene divergence of Ionopsidium and Cochlearia and its impact on the systematics and biogeography of the tribe Cochlearieae (Brassicaceae). Taxon *61*, 76–92.

35. Koch, M.A., Möbus, J., Klöcker, C.A., Lippert, S., Ruppert, L., and Kiefer, C. (2020). The Quaternary evolutionary history of Bristol rock cress (Arabis scabra, Brassicaceae), a Mediterranean element with an outpost in the north-western Atlantic region. Ann. Bot. *126*, 103–118.

36. Fekete, R., Mesterházy, A., Valkó, O., and Molnár, A.V. (2018). A hitchhiker from the beach: the spread of the maritime halophyte Cochlearia danica along salted continental roads. Preslia *90*, 23–37.

37. Raj, A., Stephens, M., and Pritchard, J.K. (2014). fastSTRUCTURE: variational inference of population structure in large SNP data sets. Genetics *197*, 573–589.

38. Kolmogorov, M., Yuan, J., Lin, Y., and Pevzner, P.A. (2019). Assembly of long, error-prone reads using repeat graphs. Nat. Biotechnol. *37*, 540–546.

39. Chen, Y., Nie, F., Xie, S.-Q., Zheng, Y.-F., Bray, T., Dai, Q., Wang, Y.-X., Xing, J.-f., Huang, Z.-J., and Wang, D.-P. (2020). Fast and accurate assembly of Nanopore reads via progressive error correction and adaptive read selection. Preprint at bioRxiv. https://doi.org/10.1101/2020.02.01.930107.

40. Laetsch, D.R., and Blaxter, M.L. (2017). BlobTools: Interrogation of genome assemblies. F1000Res. *6*, 1287.

41. Rhie, A., Walenz, B.P., Koren, S., and Phillippy, A.M. (2020). Merqury: reference-free quality, completeness, and phasing assessment for genome assemblies. Genome Biol. *21*, 245. https://doi.org/10.1186/s13059-020-02134-9.

42. Ranallo-Benavidez, T.R., Jaron, K.S., and Schatz, M.C. (2020). GenomeScope 2.0 and Smudgeplot for reference-free profiling of polyploid genomes. Nat. Commun. *11*, 1432. https://doi.org/10.1038/s41467-020-14998-3.

43. Manni, M., Berkeley, M.R., Seppey, M., Simão, F.A., and Zdobnov, E.M. (2021). BUSCO Update: Novel and Streamlined Workflows along with Broader and Deeper Phylogenetic Coverage for Scoring of Eukaryotic, Prokaryotic, and Viral Genomes. Mol. Biol. Evol. *38*, 4647–4654. https://doi.org/10.1093/molbev/msab199.

44. Huang, N., and Li, H. (2023). compleasm: a faster and more accurate reimplementation of BUSCO. Bioinformatics *39*, btad595. https://doi.org/10.1093/bioinformatics/btad595.

45. Brůna, T., Hoff, K.J., Lomsadze, A., Stanke, M., and Borodovsky, M. (2021). BRAKER2: automatic eukaryotic genome annotation with GeneMark-EP+ and AUGUSTUS supported by a protein database. NAR Genom. Bioinform. *3*, lqaa108.

46. Bohutínská, M., Vlček, J., Monnahan, P., and Kolář, F. (2023). Population Genomic Analysis of Diploid-Autopolyploid Species. In Polyploidy: Methods and Protocols, Y. Van de Peer, ed. (Springer US), pp. 297–324. https://doi.org/10.1007/978-1-0716-2561-3_16.

47. Konečná, V., Bray, S., Vlcek, J., Bohutinska, M., Pozarova, D., Choudhury, R.R., Bollmann-Giolai, A., Flis, P., Salt, D.E., Parisod, C., et al. (2021). Parallel adaptation in autopolyploid Arabidopsis arenosa is dominated by repeated recruitment of shared alleles. Nat. Commun. *12*, 4979. https://doi.org/10.1038/s41467-021-25256-5.

48. Monnahan, P., Kolář, F., Baduel, P., Sailer, C., Koch, J., Horvath, R., Laenen, B., Schmickl, R., Paajanen, P., Šrámková, G., et al. (2019). Pervasive population genomic consequences of genome duplication in Arabidopsis arenosa. Nat. Ecol. Evol. *3*, 457–468. https://doi.org/10.1038/s41559-019-0807-4.

49. Chao, D.Y., Dilkes, B., Luo, H., Douglas, A., Yakubova, E., Lahner, B., and Salt, D.E. (2013). Polyploids exhibit higher potassium uptake and salinity tolerance in Arabidopsis. Science *341*, 658–659. https://doi.org/10.1126/science.1240561.

50. Busoms, S., Fischer, S., and Yant, L. (2023). Chasing the mechanisms of ecologically adaptive salinity tolerance. Plant Commun. *4*, 100571. https://doi.org/10.1016/j.xplc.2023.100571.

51. Cruickshank, T.E., and Hahn, M.W. (2014). Reanalysis suggests that genomic islands of speciation are due to reduced diversity, not reduced gene flow. Mol. Ecol. *23*, 3133–3157.

52. Ronfort, J., Jenczewski, E., Bataillon, T., and Rousset, F. (1998). Analysis of population structure in autotetraploid species. Genetics *150*, 921–930.

53. Hudson, R.R., Slatkin, M., and Maddison, W.P. (1992). Estimation of levels of gene flow from DNA sequence data. Genetics *132*, 583–589.

54. Nei, M. (1972). Genetic distance between populations. Am. Nat. *106*, 283–292.

55. Weir, B.S., and Cockerham, C.C. (1984). Estimating F-statistics for the analysis of population structure. Evolution *38*, 1358–1370.

56. Bhatia, G., Patterson, N., Sankararaman, S., and Price, A.L. (2013). Estimating and interpreting FST: the impact of rare variants. Genome Res. *23*, 1514–1521.

57. Craske, B., and Welburn, J.P.I. (2020). Leaving no-one behind: how CENP-E facilitates chromosome alignment. Essays Biochem. *64*, 313–324.

58. Pisa, R., Phua, D.Y.Z., and Kapoor, T.M. (2020). Distinct Mechanisms of Resistance to a CENP-E Inhibitor Emerge in Near-Haploid and Diploid Cancer Cells. Cell Chem. Biol. *27*, 850–857.e6. https://doi.org/10.1016/j.chembiol.2020.05.003.

59. Real, A.M., Marsiglia, W.M., and Dar, A.C. (2020). Ploidy Leads a Molecular Motor to Walk Different Paths to Drug Resistance. Cell Chem. Biol. *27*, 770–772. https://doi.org/10.1016/j.chembiol.2020.06.019.

60. Yoshizawa, K., Matsura, A., Shimada, M., Ishida-Ishihara, S., Sato, F., Yamamoto, T., Yaguchi, K., Kawamoto, E., Kuroda, T., and Matsuo, K. (2023). Tetraploidy-linked sensitization to CENP-E inhibition in human cells. Mol. Oncol. *17*, 1148–1166.

61. Isono, K., Yamamoto, H., Satoh, K., and Kobayashi, H. (1999). An Arabidopsis cDNA encoding a DNA-binding protein that is highly similar to the DEAH family of RNA/DNA helicase genes. Nucleic Acids Res. *27*, 3728–3735.

62. Kim, J.S., Sakamoto, Y., Takahashi, F., Shibata, M., Urano, K., Matsunaga, S., Yamaguchi-Shinozaki, K., and Shinozaki, K. (2022). Arabidopsis TBP-ASSOCIATED FACTOR 12 ortholog NOBIRO6 controls root elongation with unfolded protein response cofactor activity. Proc. Natl. Acad. Sci. USA *119*, e2120219119. https://doi.org/10.1073/pnas.2120219119.

63. Rolly, N.K., and Yun, B.W. (2021). Regulation of Nitrate (NO(3)) Transporters and Glutamate Synthase-Encoding Genes under Drought Stress in Arabidopsis: The Regulatory Role of AtbZIP62 Transcription Factor. Plants *10*, 2149. https://doi.org/10.3390/plants10102149.

64. Iemura, K., and Tanaka, K. (2015). Chromokinesin Kid and kinetochore kinesin CENP-E differentially support chromosome congression without end-on attachment to microtubules. Nat. Commun. *6*, 6447. https://doi.org/10.1038/ncomms7447.

65. Fellmeth, J.E., and McKim, K.S. (2020). Meiotic CENP-C is a shepherd: bridging the space between the centromere and the kinetochore in time and space. Essays Biochem. *64*, 251–261. https://doi.org/10.1042/EBC20190080.

66. Ogura, Y., Shibata, F., Sato, H., and Murata, M. (2004). Characterization of a CENP-C homolog in Arabidopsis thaliana. Genes Genet. Syst. *79*, 139–144.

67. Hamasaki, H., Yoshizumi, T., Takahashi, N., Higuchi, M., Kuromori, T., Imura, Y., Shimada, H., and Matsui, M. (2012). SD3, an Arabidopsis thaliana homolog of TIM21, affects intracellular ATP levels and seedling development. Mol. Plant *5*, 461–471. https://doi.org/10.1093/mp/ssr088.

68. Sakamoto, T., Inui, Y.T., Uraguchi, S., Yoshizumi, T., Matsunaga, S., Mastui, M., Umeda, M., Fukui, K., and Fujiwara, T. (2011). Condensin II alleviates DNA damage and is essential for tolerance of boron overload stress in Arabidopsis. Plant Cell *23*, 3533–3546. https://doi.org/10.1105/tpc.111.086314.

69. Municio, C., Antosz, W., Grasser, K.D., Kornobis, E., Van Bel, M., Eguinoa, I., Coppens, F., Bräutigam, A., Lermontova, I., Bruckmann, A., et al. (2021). The Arabidopsis condensin CAP-D subunits arrange interphase chromatin. New Phytol. *230*, 972–987. https://doi.org/10.1111/nph.17221.

70. Wood, J.L., Liang, Y., Li, K., and Chen, J. (2008). Microcephalin/MCPH1 associates with the condensin II complex to function in homologous recombination repair. J. Biol. Chem. *283*, 29586–29592.

71. Busoms, S., Paajanen, P., Marburger, S., Bray, S., Huang, X.Y., Poschenrieder, C., Yant, L., and Salt, D.E. (2018). Fluctuating selection on migrant adaptive sodium transporter alleles in coastal Arabidopsis thaliana. Proc. Natl. Acad. Sci. USA *115*, E12443–E12452. https://doi.org/10.1073/pnas.1816964115.

72. Barrada, A., Djendli, M., Desnos, T., Mercier, R., Robaglia, C., Montané, M.-H., and Menand, B. (2019). A TOR-YAK1 signaling axis controls cell

cycle, meristem activity and plant growth in Arabidopsis. Development *146*, dev171298.

73. Kim, D., Ntui, V.O., and Xiong, L. (2016). Arabidopsis YAK 1 regulates abscisic acid response and drought resistance. FEBS Lett. *590*, 2201–2209.
74. Komaki, S., Takeuchi, H., Hamamura, Y., Heese, M., Hashimoto, T., and Schnittger, A. (2020). Functional Analysis of the Plant Chromosomal Passenger Complex. Plant Physiol. *183*, 1586–1599. https://doi.org/10.1104/pp.20.00344.
75. Kirioukhova, O., Johnston, A.J., Kleen, D., Kägi, C., Baskar, R., Moore, J.M., Bäumlein, H., Gross-Hardt, R., and Grossniklaus, U. (2011). Female gametophytic cell specification and seed development require the function of the putative Arabidopsis INCENP ortholog WYRD. Development *138*, 3409–3420. https://doi.org/10.1242/dev.060384.
76. Szpak, M., Mezzavilla, M., Ayub, Q., Chen, Y., Xue, Y., and Tyler-Smith, C. (2018). FineMAV: prioritizing candidate genetic variants driving local adaptations in human populations. Genome Biol. *19*, 1–18.
77. Diaz, K.J. (2014). A novel kinesin, Arabidopsis thaliana Centromere associated protein E2, is necessary for the progression of mitosis and meiosis (University of Massachusetts Boston).
78. She, Z.Y., Yu, K.W., Zhong, N., Xiao, Y., Wei, Y.L., Lin, Y., Li, Y.L., and Lu, M.H. (2020). Kinesin-7 CENP-E regulates chromosome alignment and genome stability of spermatogenic cells. Cell Death Dis. *6*, 25. https://doi.org/10.1038/s41420-020-0261-8.
79. Wood, K.W., Lad, L., Luo, L., Qian, X., Knight, S.D., Nevins, N., Brejc, K., Sutton, D., Gilmartin, A.G., Chua, P.R., et al. (2010). Antitumor activity of an allosteric inhibitor of centromere-associated protein-E. Proc. Natl. Acad. Sci. USA *107*, 5839–5844. https://doi.org/10.1073/pnas.0915068107.
80. Matsuo, K., and Tamaoki, N. (2021). Rational design and development of a lit-active photoswitchable inhibitor targeting CENP-E. Org. Biomol. Chem. *19*, 6979–6984. https://doi.org/10.1039/d1ob01332g.
81. Marx, A., Hoenger, A., and Mandelkow, E. (2009). Structures of kinesin motor proteins. Cell Motil Cytoskeleton *66*, 958–966.
82. Mirzaa, G.M., Vitre, B., Carpenter, G., Abramowicz, I., Gleeson, J.G., Paciorkowski, A.R., Cleveland, D.W., Dobyns, W.B., and O'Driscoll, M. (2014). Mutations in CENPE define a novel kinetochore-centromeric mechanism for microcephalic primordial dwarfism. Hum. Genet. *133*, 1023–1039.
83. Yen, T.J., Li, G., Schaar, B.T., Szilak, I., and Cleveland, D.W. (1992). CENP-E is a putative kinetochore motor that accumulates just before mitosis. Nature *359*, 536–539.
84. Huang, Y., Lin, L., Liu, X., Ye, S., Yao, P.Y., Wang, W., Yang, F., Gao, X., Li, J., Zhang, Y., et al. (2019). BubR1 phosphorylates CENP-E as a switch enabling the transition from lateral association to end-on capture of spindle microtubules. Cell Res. *29*, 562–578.
85. Kim, Y., Holland, A.J., Lan, W., and Cleveland, D.W. (2010). Aurora kinases and protein phosphatase 1 mediate chromosome congression through regulation of CENP-E. Cell *142*, 444–455.
86. Nousiainen, M., Silljé, H.H.W., Sauer, G., Nigg, E.A., and Körner, R. (2006). Phosphoproteome analysis of the human mitotic spindle. Proc. Natl. Acad. Sci. USA *103*, 5391–5396.
87. Espeut, J., Gaussen, A., Bieling, P., Morin, V., Prieto, S., Fesquet, D., Surrey, T., and Abrieu, A. (2008). Phosphorylation relieves autoinhibition of the kinetochore motor CENP-E. Mol. Cell *29*, 637–643.
88. Killinger, K., Böhm, M., Steinbach, P., Hagemann, G., Blüggel, M., Jänen, K., Hohoff, S., Bayer, P., Herzog, F., and Westermann, S. (2020). Auto-inhibition of Mif2/CENP-C ensures centromere-dependent kinetochore assembly in budding yeast. EMBO J. *39*, e102938. https://doi.org/10.15252/embj.2019102938.
89. Vagnarelli, P., and Earnshaw, W.C. (2004). Chromosomal passengers: the four-dimensional regulation of mitotic events. Chromosoma *113*, 211–222.
90. Smith, S.J., Osman, K., and Franklin, F.C.H. (2014). The condensin complexes play distinct roles to ensure normal chromosome morphogenesis during meiotic division in A rabidopsis. Plant J. *80*, 255–268.
91. Sakamoto, T., Sugiyama, T., Yamashita, T., and Matsunaga, S. (2019). Plant condensin II is required for the correct spatial relationship between centromeres and rDNA arrays. Nucleus *10*, 116–125.
92. Bundock, P., and Hooykaas, P. (2005). An Arabidopsis hAT-like transposase is essential for plant development. Nature *436*, 282–284.
93. Chang, W.-C., Wang, Y.-K., Liu, P.-F., Tsai, Y.-F., Kong, L.-R., Lin, C.-K., Yang, C.-H., and Pan, R.-L. (2008). Regulation of Ku gene promoters in Arabidopsis by hormones and stress. Funct. Plant Biol. *35*, 265–280.
94. Tamura, K., Adachi, Y., Chiba, K., Oguchi, K., and Takahashi, H. (2002). Identification of Ku70 and Ku80 homologues in Arabidopsis thaliana: evidence for a role in the repair of DNA double-strand breaks. Plant J. *29*, 771–781.
95. Li, S., Ding, B., Chen, R., Ruggiero, C., and Chen, X. (2006). Evidence that the transcription elongation function of Rpb9 is involved in transcription-coupled DNA repair in Saccharomyces cerevisiae. Mol. Cell Biol. *26*, 9430–9441.
96. Hull, M.W., McKune, K., and Woychik, N.A. (1995). RNA polymerase II subunit RPB9 is required for accurate start site selection. Genes Dev. *9*, 481–490.
97. Tan, E.H., Blevins, T., Ream, T.S., and Pikaard, C.S. (2012). Functional consequences of subunit diversity in RNA polymerases II and V. Cell Rep. *1*, 208–214.
98. Hemming, S.A., Jansma, D.B., Macgregor, P.F., Goryachev, A., Friesen, J.D., and Edwards, A.M. (2000). RNA polymerase II subunit Rpb9 regulates transcription elongation in vivo. J. Biol. Chem. *275*, 35506–35511.
99. Nesser, N.K., Peterson, D.O., and Hawley, D.K. (2006). RNA polymerase II subunit Rpb9 is important for transcriptional fidelity in vivo. Proc. Natl. Acad. Sci. USA *103*, 3268–3273.
100. Allen, B.L., and Taatjes, D.J. (2015). The Mediator complex: a central integrator of transcription. Nat. Rev. Mol. Cell Biol. *16*, 155–166.
101. Baxter, I., Brazelton, J.N., Yu, D., Huang, Y.S., Lahner, B., Yakubova, E., Li, Y., Bergelson, J., Borevitz, J.O., Nordborg, M., et al. (2010). A coastal cline in sodium accumulation in Arabidopsis thaliana is driven by natural variation of the sodium transporter AtHKT1; 1. PLoS Genet. *6*, e1001193.
102. Shi, H., Ishitani, M., Kim, C., and Zhu, J.-K. (2000). The Arabidopsis thaliana salt tolerance gene SOS1 encodes a putative Na+/H+ antiporter. Proc. Natl. Acad. Sci. USA *97*, 6896–6901.
103. Zhou, M., and Wang, W. (2022). SOS1 safeguards plant circadian rhythm against daily salt fluctuations. Proc. Natl. Acad. Sci. USA *119*, e2212950119. https://doi.org/10.1073/pnas.2212950119.
104. Furini, S., and Domene, C. (2013). K+ and Na+ conduction in selective and nonselective ion channels via molecular dynamics simulations. Biophys. J. *105*, 1737–1745.
105. Cotsaftis, O., Plett, D., Shirley, N., Tester, M., and Hrmova, M. (2012). A two-staged model of Na+ exclusion in rice explained by 3D modeling of HKT transporters and alternative splicing. PLoS One *7*, e39865.
106. Almeida, P., Katschnig, D., and De Boer, A.H. (2013). HKT transporters—state of the art. Int. J. Mol. Sci. *14*, 20359–20385.
107. Wang, Y., Pan, C., Chen, Q., Xie, Q., Gao, Y., He, L., Li, Y., Dong, Y., Jiang, X., and Zhao, Y. (2023). Architecture and autoinhibitory mechanism of the plasma membrane Na+/H+ antiporter SOS1 in Arabidopsis. Nat. Commun. *14*, 4487.
108. Pandey, A.K., Ganguly, H.K., Sinha, S.K., Daniels, K.E., Yap, G.P., Patel, S., and Zondlo, N.J. (2023). An Inherent Difference between Serine and Threonine Phosphorylation: Phosphothreonine Strongly Prefers a Highly Ordered, Compact, Cyclic Conformation. ACS Chem. Biol. *18*, 1938–1958.
109. Kant, P., Kant, S., Gordon, M., Shaked, R., and Barak, S. (2007). STRESS RESPONSE SUPPRESSOR1 and STRESS RESPONSE SUPPRESSOR2,

two DEAD-box RNA helicases that attenuate Arabidopsis responses to multiple abiotic stresses. Plant Physiol. *145*, 814–830.

110. Khan, A., Garbelli, A., Grossi, S., Florentin, A., Batelli, G., Acuna, T., Zolla, G., Kaye, Y., Paul, L.K., Zhu, J.K., et al. (2014). The A rabidopsis STRESS RESPONSE SUPPRESSOR DEAD-box RNA helicases are nucleolar-and chromocenter-localized proteins that undergo stress-mediated relocalization and are involved in epigenetic gene silencing. Plant J. *79*, 28–43.

111. Kim, J.S., Kim, K.A., Oh, T.R., Park, C.M., and Kang, H. (2008). Functional characterization of DEAD-box RNA helicases in Arabidopsis thaliana under abiotic stress conditions. Plant Cell Physiol. *49*, 1563–1571.

112. Nawaz, I., Iqbal, M., Bliek, M., and Schat, H. (2017). Salt and heavy metal tolerance and expression levels of candidate tolerance genes among four extremophile Cochlearia species with contrasting habitat preferences. Sci. Total Environ. *584–585*, 731–741. https://doi.org/10.1016/j.scitotenv.2017.01.111.

113. Emms, D.M., and Kelly, S. (2018). OrthoFinder2: fast and accurate phylogenomic orthology analysis from gene sequences. Preprint at bioRxiv, 466201. https://doi.org/10.1101/466201.

114. Sterken, R., Kiekens, R., Boruc, J., Zhang, F., Vercauteren, A., Vercauteren, I., De Smet, L., Dhondt, S., Inzé, D., De Veylder, L., et al. (2012). Combined linkage and association mapping reveals CYCD5;1 as a quantitative trait gene for endoreduplication in Arabidopsis. Proc. Natl. Acad. Sci. USA *109*, 4678–4683.

115. Wang, M., Zhao, Y., and Zhang, B. (2015). Efficient Test and Visualization of Multi-Set Intersections. Sci. Rep. *5*, 16923. https://doi.org/10.1038/srep16923.

116. Szklarczyk, D., Gable, A.L., Lyon, D., Junge, A., Wyder, S., Huerta-Cepas, J., Simonovic, M., Doncheva, N.T., Morris, J.H., Bork, P., et al. (2019). STRING v11: protein–protein association networks with increased coverage, supporting functional discovery in genome-wide experimental datasets. Nucleic Acids Res. *47*, D607–D613.

117. Bomblies, K. (2023). Learning to tango with four (or more): the molecular basis of adaptation to polyploid meiosis. Plant Reprod. *36*, 107–124. https://doi.org/10.1007/s00497-022-00448-1.

118. Levin, D.A. (1983). Polyploidy and Novelty in Flowering Plants. Am. Nat. *122*, 1–25. https://doi.org/10.1086/284115.

119. Bomblies, K., Higgins, J.D., and Yant, L. (2015). Meiosis evolves: adaptation to external and internal environments. New Phytol. *208*, 306–323. https://doi.org/10.1111/nph.13499.

120. Unhavaithaya, Y., and Orr-Weaver, T.L. (2013). Centromere proteins CENP-C and CAL1 functionally interact in meiosis for centromere clustering, pairing, and chromosome segregation. Proc. Natl. Acad. Sci. USA *110*, 19878–19883.

121. Kurzbauer, M.-T., Janisiw, M.P., Paulin, L.F., Prusén Mota, I., Tomanov, K., Krsicka, O., Haeseler, A.v., Schubert, V., and Schlögelhofer, P. (2021). ATM controls meiotic DNA double-strand break formation and recombination and affects synaptonemal complex organization in plants. Plant Cell *33*, 1633–1656.

122. Bonnet, S., Knoll, A., Hartung, F., and Puchta, H. (2013). Different functions for the domains of the Arabidopsis thaliana RMI1 protein in DNA cross-link repair, somatic and meiotic recombination. Nucleic Acids Res. *41*, 9349–9360.

123. Eisenschmid, K., Jabbusch, S., and Koch, M.A. (2023). Evolutionary footprints of cold adaptation in arctic-alpine Cochlearia (Brassicaceae)–Evidence from freezing experiments and electrolyte leakage. Perspect. Plant Ecol. Evol. Systemat. *59*, 125728.

124. Deorowicz, S., Debudaj-Grabysz, A., and Grabowski, S. (2013). Disk-based k-mer counting on a PC. BMC Bioinf. *14*, 1–12.

125. Oxford Nanopore Techologies. medaka: Sequence correction provided by ONT Research. http://github.com/nanoporetech/medaka, accessed February 14, 2023

126. Walker, B.J., Abeel, T., Shea, T., Priest, M., Abouelliel, A., Sakthikumar, S., Cuomo, C.A., Zeng, Q., Wortman, J., Young, S.K., and Earl, A.M. (2014). Pilon: an integrated tool for comprehensive microbial variant detection and genome assembly improvement. PLoS One *9*, e112963.

127. Bolger, A.M., Lohse, M., and Usadel, B. (2014). Trimmomatic: a flexible trimmer for Illumina sequence data. Bioinformatics *30*, 2114–2120.

128. Li, H. (2013). Aligning sequence reads, clone sequences and assembly contigs with BWA-MEM. Preprint at arXiv. https://doi.org/10.48550/arXiv.1303.3997.

129. Dudchenko, O., Batra, S.S., Omer, A.D., Nyquist, S.K., Hoeger, M., Durand, N.C., Shamim, M.S., Machol, I., Lander, E.S., Aiden, A.P., and Aiden, E.L. (2017). De novo assembly of the Aedes aegypti genome using Hi-C yields chromosome-length scaffolds. Science *356*, 92–95.

130. Durand, N.C., Robinson, J.T., Shamim, M.S., Machol, I., Mesirov, J.P., Lander, E.S., and Aiden, E.L. (2016). Juicebox provides a visualization system for Hi-C contact maps with unlimited zoom. Cell Syst. *3*, 99–101.

131. Novák, P., Neumann, P., Pech, J., Steinhaisl, J., and Macas, J. (2013). RepeatExplorer: a Galaxy-based web server for genome-wide characterization of eukaryotic repetitive elements from next-generation sequence reads. Bioinformatics *29*, 792–793.

132. Ou, S., Su, W., Liao, Y., Chougule, K., Ware, D., Peterson, T., Jiang, N., Hirsch, C., and Hufford, M. (2019). Benchmarking transposable element annotation methods for creation of a streamlined. Genome Biol. *20*, 1–18.

133. Dobin, A., Davis, C.A., Schlesinger, F., Drenkow, J., Zaleski, C., Jha, S., Batut, P., Chaisson, M., and Gingeras, T.R. (2013). STAR: ultrafast universal RNA-seq aligner. Bioinformatics *29*, 15–21.

134. Li, H., and Durbin, R. (2009). Fast and accurate short read alignment with Burrows–Wheeler transform. Bioinformatics *25*, 1754–1760.

135. Li, H., Handsaker, B., Wysoker, A., Fennell, T., Ruan, J., Homer, N., Marth, G., Abecasis, G., and Durbin, R.; 1000 Genome Project Data Processing Subgroup (2009). The sequence alignment/map format and SAMtools. Bioinformatics *25*, 2078–2079.

136. McKenna, A., Hanna, M., Banks, E., Sivachenko, A., Cibulskis, K., Kernytsky, A., Garimella, K., Altshuler, D., Gabriel, S., Daly, M., and DePristo, M.A. (2010). The Genome Analysis Toolkit: a MapReduce framework for analyzing next-generation DNA sequencing data. Genome Res. *20*, 1297–1303.

137. Patterson, N., Price, A.L., and Reich, D. (2006). Population structure and eigenanalysis. PLoS Genet. *2*, e190.

138. Pembleton, L.W., Cogan, N.O.I., and Forster, J.W. (2013). St AMPP: An R package for calculation of genetic differentiation and structure of mixed-ploidy level populations. Mol. Ecol. Resour. *13*, 946–952.

139. Huson, D.H. (1998). SplitsTree: analyzing and visualizing evolutionary data. Bioinformatics *14*, 68–73.

140. Gerard, D. (2021). Pairwise linkage disequilibrium estimation for polyploids. Mol. Ecol. Resour. *21*, 1230–1242.

141. Alexa, A., and Rahnenführer, J. (2009). Gene set enrichment analysis with topGO. Bioconductor Improv *27*, 1–26.

142. Sievers, F., and Higgins, D.G. (2014). Clustal omega. Curr. Protoc. Bioinformatics *48*, 3–13.

143. Waterhouse, A.M., Procter, J.B., Martin, D.M.A., Clamp, M., and Barton, G.J. (2009). Jalview Version 2—a multiple sequence alignment editor and analysis workbench. Bioinformatics *25*, 1189–1191.

144. Jumper, J., Evans, R., Pritzel, A., Green, T., Figurnov, M., Ronneberger, O., Tunyasuvunakool, K., Bates, R., Žídek, A., Potapenko, A., et al. (2021). Highly accurate protein structure prediction with AlphaFold. Nature *596*, 583–589.

145. Desjardins, S., Kanyuka, K., and Higgins, J.D. (2020). A cytological analysis of wheat meiosis targeted by virus-induced gene silencing (VIGS). Methods Mol. Biol. *2061*, 319–330.

146. Higgins, J.D., Sanchez-Moran, E., Armstrong, S.J., Jones, G.H., and Franklin, F.C.H. (2005). The Arabidopsis synaptonemal complex protein

ZYP1 is required for chromosome synapsis and normal fidelity of crossing over. Genes Dev. *19*, 2488–2500.

147. Desjardins, S.D., Ogle, D.E., Ayoub, M.A., Heckmann, S., Henderson, I.R., Edwards, K.J., and Higgins, J.D. (2020). MutS homologue 4 and MutS homologue 5 maintain the obligate crossover in wheat despite stepwise gene loss following polyploidization. Plant Physiol. *183*, 1545–1558.

148. Mandáková, T., and Lysak, M.A. (2016). Chromosome preparation for cytogenetic analyses in Arabidopsis. Curr. Protoc. Plant Biol. *1*, 43–51.

149. Ijdo, J.W., Wells, R.A., Baldini, A., and Reeders, S.T. (1991). Improved telomere detection using a telomere repeat probe (TTAGGG) n generated by PCR. Nucleic Acids Res. *19*, 4780.

150. Mandáková, T., Kovarik, A., Zozomová-Lihová, J., Shimizu-Inatsugi, R., Shimizu, K.K., Mummenhoff, K., Marhold, K., and Lysak, M.A. (2013). The more the merrier: recent hybridization and polyploidy in cardamine. Plant Cell *25*, 3280–3295. https://doi.org/10.1105/tpc.113.114405.

151. Mandáková, T., and Lysak, M.A. (2016). Painting of Arabidopsis chromosomes with chromosome-specific BAC clones. Curr. Protoc. Plant Biol. *1*, 359–371.

STAR★METHODS

KEY RESOURCES TABLE

REAGENT or RESOURCE	SOURCE	IDENTIFIER
Antibodies		
Rat anti-ZYP1C	Higgins et al.[124]	N/A
Rabbit anti-HEI10	Desjardins et al.[125]	N/A
Goat anti-rat Alexa Fluor® 594	Thermofisher Scientific	A48264
Goat anti-rabbit Alexa Fluor® 488	Thermofisher Scientific	A-11008
Biological samples		
Cochlearia excelsa	This paper	Biosample in https://www.ebi.ac.uk/ena/browser/view/PRJEB66308
Cochlearia pyrenaica	This paper	Biosample in https://www.ebi.ac.uk/ena/browser/view/PRJEB66308
Cochlearia officinalis	This paper	Biosample in https://www.ebi.ac.uk/ena/browser/view/PRJEB66308
Cochlearia danica	This paper	Biosample in https://www.ebi.ac.uk/ena/browser/view/PRJEB66308
Ionopsidium spp.	This paper	Biosample in https://www.ebi.ac.uk/ena/browser/view/PRJEB66308
Chemicals, peptides, and recombinant proteins		
CTAB - Lysis buffer BioChemica	ITW Reagents	A4150
Proteinase K	Qiagen	19131
RNaseA	Qiagen	19101
Phenol:chloroform:isoamyl-alcohol	Sigma	77617-500ML
Chloroform	Fisher Scientific	C/4960/PB17
Ethanol	Honeywell	32221-2.5L
Sodium Acetatate (NaOAc) 3M	Sigma	S7899
Nuclease free water	Sigma	W4502
NEBNext Ultra II End repair/dA-tailing Module	New England Biolabs	E7546
NEBNext FFPE Repair Mix	New England Biolabs	M6630
NEBNext Quick Ligation Module	New England Biolabs	E6056
NEB Blunt/TA Ligase Master Mix	New England Biolabs	M0367
2-Mercapthoethanol, $\geq$ 98%	Sigma-Aldrich	M3148
3-Amino-3-Deoxydigoxigenin Hemisuccinamide, Succinimidyl Ester	Invitrogen™	A2952
4′,6-Diamidino-2-phenylindole dihydrochloride	Sigma-Aldrich	D8417
Acetic acid 99%	Penta	20000–11000
Agarose	Sigma-Aldrich	A9539
Albumin bovine Fraction V, pH 7.0 (BSA)	Serva	11930
Alexa Fluor™ 488 NHS Ester (Succinimidyl Ester)	Invitrogen™	A20000
Alexa Fluor™ 546 NHS Ester (Succinimidyl Ester)	Invitrogen™	A20002
Alexa Fluor™ 594 NHS Ester (Succinimidyl Ester)	Invitrogen™	A37565
Alexa Fluor™ 647-aha-dUTP, 1 mM in TE buffer	Invitrogen™	A32763
Aminoallyl-dUTP sodium salt	Sigma-Aldrich	A0410

(*Continued on next page*)

Continued

REAGENT or RESOURCE	SOURCE	IDENTIFIER
Aminoallyl-dUTP, 10 mM	BIORON	513001
Anti-DNP antibody produced in rabbit	Sigma-Aldrich	D9656
BIOTIN – NICK TRANSLATION MIX	Roche	11745824910
Biotin-XX, SE (6-Biotinoyl Amino Hexanoic Acid, Succinimidyl Ester)	Invitrogen™	B1606
Blocking Reagent	Roche	11096176001
Cellulase from Trichoderma sp.	Sigma-Aldrich	C1794
Citric acid	Penta	18790–31000
Cy3 Mono NHS Ester	Amersham	PA13104
Cytohelicase from Heix pomatia	Sigma-Aldrich	C8274
dATP Li-salt, (2′-Deoxyadenosine 5′-triphosphate sodium salt solution)	Roche	11051440001
dCTP Li-salt, (, 2′-deoxy-cytidine-5′-triphosphate)	Roche	11051458001
Dextran sulfate sodium salt from Leuconostoc spp.	Sigma-Aldrich	D8906
dGTP Li-salt, 2′-Deoxyguanosine 5′-triphosphate trisodium salt solution)	Roche	11051466001
DIG – NICK TRANSLATION MIX	Roche	11745816910
Dimethyl sulfoxide ≥99,9%, for molecular biology	Sigma-Aldrich	D8418
DNA Gel Loading Dye (6X)	Thermo Scientific™	R0611
DNA Polymerase I (10 U/μL)	Thermo Scientific™	EP0042
Dnase I, (Deoxyribonuclease)	Roche	10104159001
DNP-X, SE, 6-(2,4-Dinitrophenyl) aminohexanoic Acid, Succinimidyl Ester	Invitrogen™	D-2248
dTTP Li-salt, (2′-deoxy-thymidine-5′-triphosphate)	Roche	11051482001
Ethanol 70%	Penta	70392–11002
Ethanol 96% (sazba SD 285,-)	Penta	70390–11000
Ethanol absolute	Penta	71250–11002
Ethylenediaminetetraacetic acid disodium salt dihydrate	Sigma-Aldrich	E5134
Formaldehyde solution ACS reagent 37%	Sigma-Aldrich	252549
Formamide (Deionized)	Invitrogen™	AM9342
Formamide 100%	Penta	14190–11000
GelRed® Nucleic Acid Gel Stain	Biotium	41003
GeneRuler 100 bp DNA Ladder	Thermo Scientific™	SM0242
Glycerol anhydrous	Penta	14550-11000PE
Glycine, BioXtra, ≥99% (titration)	Sigma-Aldrich	G7403
Goat Anti-Avidin D Antibody, Biotinylated	VectorLaboratories	BA-0300-.5
Goat anti-Mouse IgG (H + L) Cross-Adsorbed Secondary Antibody, Alexa Fluor™ 488	Invitrogen™	A-11001
Hydrochloric acid	Penta	19360–11000
ChromaTide™ Alexa Fluor™ 488-5-dUTP	Invitrogen™	C11397
ChromaTide™ Alexa Fluor™ 546-14-dUTP	Invitrogen™	C11401
ChromaTide™ Alexa Fluor™ 594-5-dUTP	Invitrogen™	C11400
IgG Fraction Monoclonal Mouse Anti-Digoxin	JacksonImmunoResearch	200-002-156
Magnesium chloride hexahydrate	Sigma-Aldrich	M2670

(*Continued on next page*)

Continued

REAGENT or RESOURCE	SOURCE	IDENTIFIER
Nick Translation Mix	Roche	11745808910
Pectolyase Y – 23	Duchefa	P8004
Pepsin, from porcine gastric mucosa	Sigma-Aldrich	P6887
Potassium hydroxide	Penta	15520–31000
Propyl gallate	Sigma-Aldrich	48710
Ready-to-use 100 bp DNA ladder	Biotium	31032
Ribonuclease A (RNase) Dnase free	PanReac AppliChem	A3832
SDS BioChemica	Applichem	A2572
Sodium acetate anhydrous, ≥99%	Sigma-Aldrich	S2889
Sodium bicarbonate	Penta	15350–31000
Sodium citrate	Penta	11470–31000
Sodium hydroxide	Penta	15760–31000
Sodium chloride	Penta	16610–31000
Texas Red™ Avidin D	VectorLaboratories	A-2006-5
Tris for analysis, ACS, ultrapure	Applichem	A1086
TWEEN® 20	Sigma-Aldrich	P1379
VECTASHIELD® Antifade Mounting Medium	VectorLaboratories	H-1000-10
Critical commercial assays		
Short Read Eliminator XS	Pacific Biosciences	SKU 102-208-200
AMPure XP	Beckman Coulter	A63882
Genomic DNA ScreenTape Reagents	Agilent	5067–5366
Genomic DNA ScreenTape	Agilent	5067–5365
Qubit dsDNA HS Assay Kit	Thermo Fisher Scientific	Q32851
Ligation Sequencing Kit (gDNA)	Oxford Nanopore Technologies (ONT)	SQK-LSK109
Native Barcoding Expansion kit	ONT	EXP-NBD196
Flow Cell Wash Kit	ONT	EXP-WSH002
Flow Cell (R9.4.1)	ONT	FLO-MIN106D
Deposited data		
Raw data of genome sequencing.	European Nucleotide Archive	Accession number PRJEB66308. https://www.ebi.ac.uk/ena/browser/view/PRJEB66308
Genome assembly and annotation.	Data Dryad	https://doi.org/10.1101/2023.09.27.559727. https://doi.org/10.5061/dryad.ncjsxkt1s
Software and algorithms		
KMC 3.2.4	Deorowicz et al.[126]	https://github.com/refresh-bio/KMC
GenomeScope 2.0	Ranallo-Benavidez et al.[44]	https://github.com/tbenavi1/genomescope2.0
Smudgeplot 0.2.5	Ranallo-Benavidez et al.[44]	https://github.com/KamilSJaron/smudgeplot
Guppy 6	ONT technologies	https://nanoporetech.com/
Flye 2.9	Kolmogorov et al.[38]	https://github.com/fenderglass/Flye
Necat 0.0.1	Chen et al.[39]	https://github.com/xiaochuanle/NECAT
Medaka 1.11	Wright et al.[40]	https://github.com/nanoporetech/medaka
Pilon 1.24	Walker et al.[41]	https://github.com/broadinstitute/pilon
Trimmomatic 0.39	Bolger et al.[127]	https://github.com/usadellab/Trimmomatic
Bwa-mem 0.7	Li[128]	https://github.com/lh3/bwa
Picard 3.1	Broad Institue[129]	https://github.com/broadinstitute/picard
3D-DNA 201008	Dudchenko et al.[130]	https://github.com/aidenlab/3d-dna

(*Continued on next page*)

Continued

REAGENT or RESOURCE	SOURCE	IDENTIFIER
Juicebox 2.20.00	Durand et al.[131]	https://github.com/aidenlab/Juicebox
RepeatExplorer2	Novák et al.[132]	https://github.com/sebhtml/RepeatExplorer
BLAST	Altschul et al.[133]	https://github.com/blast-io/blast
Blobtools 4.3	Laetsch et al.[42]	https://pypi.org/project/blobtoolkit/
BUSCO 3.0.2	Seppey et al.[46]	https://busco.ezlab.org/
Compleasm 0.2.6	Huang et al.[46]	https://github.com/huangnengCSU/compleasm
Meryl 1.4.1	Rhie et al.[43]	https://github.com/marbl/meryl
Merqury 1.3	Rhie et al.[43]	https://github.com/marbl/merqury
QUAST 5.2.0	Gurevich et al.[134]	https://github.com/ablab/quast
Samtools 1.20	Li et al.[135]	https://github.com/samtools/samtools
Diamond 2.1.90	Buchfink et al.[136]	https://github.com/bbuchfink/diamond
EDTA 1.2.0	Ou et al.[137]	https://github.com/oushujun/EDTA
BRAKER2	Brůna et al.[47]	https://github.com/Gaius-Augustus/BRAKER
STAR 2.7.11	Dobin et al.[138]	https://github.com/alexdobin/STAR
GATK 4.2.3	McKenna et al.[139]	https://gatk.broadinstitute.org/hc/en-us
Adegenet 2.1.7	Jombard et al.[140]	https://github.com/thibautjombart/adegenet
SplitsTree 6.1.10	Huson et al.[141]	https://uni-tuebingen.de/en/fakultaeten/mathematisch-naturwissenschaftliche-fakultaet/fachbereiche/informatik/lehrstuehle/algorithms-in-bioinformatics/software/splitstree/
fastSTRUCTURE 1.0	Raj et al.[37]	https://github.com/rajanil/fastStructure
R 4.3.1	CRAN project	https://cran.r-project.org/
RStudio 2023.9.0.463	RStudio team[142]	https://github.com/rstudio/rstudio
StAMPP	Pembleton et al.[143]	https://cran.r-project.org/web/packages/StAMPP/index.html
JalView 2.11	Waterhouse et al.[144]	https://www.jalview.org/
Scantools	Monnahan et al.[51]	https://github.com/mattheatley/scantools_lite
Orthofinder v. 2.5.5	Emms et al.[63]	https://github.com/davidemms/OrthoFinder
SuperExactTest	Wang et al.[72]	https://cran.r-project.org/web/packages/SuperExactTest/
TopGO v.2.52	Alexa et al.[152]	https://bioconductor.org/packages/release/bioc/html/topGO.html
Clustal-Omega	Sievers et al.[153]	http://www.clustal.org/omega/
Alphafold 2.1	Jumper et al.[154]	https://github.com/google-deepmind/alphafold
ImageJ	NIH	NIH
Photoshop CS6	Adobe	https://www.adobe.com/
FlowJo v 10.6.1	FlowJo	https://www.flowjo.com/
Minitab v 18.1.0.0	Minitab	https://www.minitab.com/

RESOURCE AVAILABILITY

Lead contacts

Further information and requests for resources and reagents should be directed to and will be fulfilled by the lead contact, Levi Yant (leviyant@gmail.com).

Materials availability

No new materials were generated in this study.

Data and code availability

- All sequence data for this study have been deposited in the European Nucleotide Archive (ENA) at https://www.ebi.ac.uk/ena/browser/view/PRJEB66308, accession number PRJEB66308.
- All custom code is available from https://doi.org/10.5281/zenodo.12674221.
- Any additional information required to reanalyze the data reported in this work paper is available from the lead contact upon request.

EXPERIMENTAL MODEL AND STUDY PARTICIPANT DETAILS

Leaf samples of *Cochlearia* species listed in Data S1, Table S2 were collected from the at the locations indicated in Data S1, Table S2. These were grown in natural conditions without chemical fertilizer at the indicated locations over their growing seasons from 2015 to 2022. Additionally, cultivated plants were produced by sowing field-collected seeds unsterilized in petri plates filled with wet sand for one week, then transferred to pot trays filled with John Innes mix (No.1) with no additional chemical fertilizer or vernalization. Plants were grown in a glasshouse at ambient Norwich, UK (or Heidelberg, DE) spring and summer temperature (~15-25C day, ~5-10C night), or in a Conviron A1000 growth chamber (16h light from 6:00 to 20:00, temperature day: 22°C and night: 18°C). After two weeks from germination, trays were bottom-watered twice weekly.

METHOD DETAILS

Plant material

We first located 89 *Cochlearia* populations throughout Europe and collected population samplings of plants from each, aiming for at least 10 plants per population, with each sampled plant a minimum of 2 m from any other. Of these, we selected 33 geographically and ecotypically diverse representative populations for population resequencing, including the outgroup *Ionopsidium* (Data S1, Table S2). An average of 4 individuals per population were sequenced. A total of 149 individuals were initially sequenced, which was narrowed down by a cutoff of minimum average depth of 4x, leaving 113 individuals from 33 populations in the final analyzed dataset, including the outgroup *Ionopsidium*.

Ploidy determination by flow cytometry

DNA content and ploidy were inferred for populations using flow cytometry (Data S1, Table S1). Approximately 1 square cm of leaf material was diced alongside an internal reference using razor blades in 1 mL ice-cold extraction buffer (either 45 mM $MgCl_2$, 30 mM sodium citrate, 20mM MOPS, 1% Triton-100, pH 7 with NaOH for relative staining or 0.1 M citric acid, 0.5% Tween 20 for absolute measurements). The resultant slurry was then filtered through a 40-μm nylon mesh before the nuclei were stained with the addition of 1 mL staining buffer (either CyStain UV precise P [Sysmex, Fluorescence emission: 435nm–500nm] for relative ploidy, or Otto 2 buffer [0.4 M $Na_2HPO_4 \cdot 12H_2O$, Propidium iodide 50 μgmL^{-1}, RNase 50 μgmL^{-1}], for absolute DNA content). After 1 min of incubation at room temperature, the sample was run for 5,000 particles on either a Partec PA II flow cytometer or a BD FACS Melody. Histograms were evaluated using FlowJo software version 10.6.1.

HEI10 immunostaining

Pachytene chromosome spreads were prepared from fixed immature anthers, through partial enzymatic digestion (1% cellulase R-10 [Duchefa] and 1% pectolyase [MP Biomedicals] in 0.01M citrate buffer), and cell spreading was performed in 70% acetic acid.[145] Immunostaining was conducted using two primary antibodies: anti-AtZYP1C rat, 1:500[146] and anti-HvHEI10 rabbit, 1:250,[147] followed by two secondary antibodies: goat anti-rat Alexa Fluor 594 (Invitrogen) and goat anti-rabbit Alexa Fluor 488 (Invitrogen). A Nikon Eclipse Ci fluorescence microscope equipped with NIS elements software was used to capture and quantify images. HEI10 foci were counted at pachytene using NIS software and significance was established using the Mann-Whitney U test (Minitab v 18.1.0.0).

Chromosome number determination, meiotic stability estimation, and fluorescence *in situ* hybridization

Mitotic and meiotic metaphase I chromosome spreads from fixed root tips and anthers, respectively, were prepared.[148] In 13 and 11 individuals, 12 and 24 chromosomes were detected within mitotic chromosome spreads. In addition to the autosomes, smaller supernumerary B chromosomes were identified as follows: LAB_201: $2n = 12 + 4B$; LAB_210: $2n = 12 + 2B$; NEN_201: $2n = 12 + 2B$; NEN_202: $2n = 12 + 4B$; NEN_203: $2n = 12 + 5B$; NEN_204: $2n = 12 + 2B$; NEN_205: $2n = 12 + 3B$; NEN_206: $2n = 12 + 3B$; NEN_207: $2n = 12 + 3B$; NEN_208: $2n = 12 + 5B$; NEN_209: $2n = 12 + 4B$; NEN_211: $2n = 12 + 2B$; NEN_212: $2n = 12$; no Bs; ROT_201: $2n = 24 + 2B$; ROT_204: $2n = 24 + 7B$; ROT_205: $2n = 24 + 3B$; ROT_208: $2n = 24 + 13B$?; ROT_210: $2n = 24 + 10B$; SKN_201: $2n = 24 + 7B$; SKN_202: $2n = 24 + 8B$; SKN_207: $2n = 24 + 3B$; SKN_209: $2n = 24 + 4B$; SKN_210: $2n = 24 + 9B$; SKN_211: $2n = 24 + 3B$. However, B chromosomes were not considered in the further analyses. Chromosome stability was assessed in DAPI-stained metaphase I in 13

individuals from two diploid populations and 11 individuals from two tetraploid populations. In diploids, spreads with 6 bivalents were categorized as "stable meiosis", 5-4 as "rather stable", 3 as "rather unstable", and less than 3 bivalents as "unstable". In tetraploids, spreads with 12 bivalents were classified as "stable meiosis", 11-9 as "rather stable", 8-6 as "rather unstable", and less than 6 bivalents as "unstable". The Arabidopsis-type telomere repeat (TTTAGGG)*n* was prepared according to.[149] The *Cochlearia*-specific 102-bp (GTTAGATGTTTCATAAGTTCGTCAA ACTTGTACAAAGCTCATTGAGACACTTATAAGCACTCATGTTGCATGAAACTTGGTT TAGAGTCCTAGAAACGCGTT) tandem repeat was designed and prepared based on[6,150] and used for identification of centromeres. The DNA probes were labeled by nick translation with biotin-dUTP and digoxigenin-dUTP according to,[151] pooled and precipitated by adding 1/10 volume of 3 M sodium acetate, pH 5.2, and 2.5 volumes of ice-cold 96% ethanol and kept at −20°C for 30 min. The pellet was then centrifuged at 13,000 g at 4°C for 30 min. The pellet was resuspended in 20 μL of the hybridization mix (50% formamide and 10% dextran sulfate in 2×SSC) per slide. 20 μL of the probe was pipetted onto a chromosome-containing slide. The coverslips were framed with rubber cement. The probe and chromosomes were denatured together on a hot plate at 80°C for 2 min and incubated in a moist chamber at 37°C overnight. Post-hybridization washing was performed according to.[151] After immunodetection, chromosomes were counterstained with 4′, 6-diamidino-2-phenylindole (DAPI, 2 μg/mL) in Vectashield (Vector Laboratories). The preparations were photographed using a Zeiss Axioimager Z2 epifluorescence microscope with a CoolCube camera (MetaSystems). The three monochromatic images were pseudocolored, merged and cropped using Photoshop CS (Adobe Systems) and ImageJ (National Institutes of Health) software.

Salinity tolerance experiments

Seeds were sowed in petri plates filled with wet sand for a week, then transferred to pot trays filled with John Innes mix (No.1). Each tray contained 60 plants. A total of 1,036 plants were planted. The experiment was conducted in complete randomized design with as many replications as possible per maternal seed line (average 13.05) and plants were grown in a glasshouse at ambient UK summer temperature (~25°C day, ~10°C night). After two weeks from germination, trays were bottom-watered twice weekly with watering solution containing either 10 mM MES pH 7 and NaCl for the treatment or just 10 mM MES for the control. Salt concentrations began at 50 mM NaCl for two weeks, then were increased to 300 mM for two weeks, and were finally increased to 600 mM for 4 weeks. During the final week, leaves were sprayed with 600 mM NaCl watering solution twice. After 8 total weeks of treatment, a modified Standard Evaluation System (SES) Score was used to evaluate symptoms of salt stress. Three individuals independently took measurements for each plant and the final score was given as the average of the three. At the same time point, two leaves of each plant were harvested, dried at 60°C for two days and stored for ICP analysis. The diploids were significantly more salt tolerant than the tetraploids (W = 29568, *p*-value = 2.178e-05, Wilcoxon rank-sum test with continuity correction performed in R Version 3.6.0).

Stomatal conductance assessment, net photosynthesis and drought tolerance experiments

To test for differences in physiological responses to drought stress we cultivated twenty different populations of *Cochlearia* side by side in a controlled environment. Seeds were germinated in wet sand in a growth camber with temperature and humidity control before being transplanted into PET-based potting soil and placed in a Conviron A1000 growth room (16h light from 6:00 to 20:00, temperature day: 22°C and night: 18°C). The watering regime for control and drought stressed plants was as follows: For the first two weeks after transplanting, they were watered 1000 mL H_2O per tray every 2nd day. From the 3rd week onwards a drought stress was imposed. Control plants were still watered with 1000 mL H_2O per tray every 2nd day. Drought stress was generated by lowering watering/soil moisture week by week as follows: week 3–1000 mL H_2O per tray every 3rd day, week 4–1000 mL H_2O per tray every 4th day, week 5–1000 mL H_2O per tray every 5th day, week 6–1000 mL H_2O per tray every 6th day. Plants were assessed at the end of week 6. Wet and dry weight of the shoot as well as photosynthesis parameters were captured. Photosynthetic parameters were assessed using the LI-6400XT Portable Photosynthesis System (LI-COR , Lincoln, NE, United States). All measurements were taken between 9:30 and 11:30 using light adapted plants. Photosynthetic parameters were measured on the largest leaf from both control and drought treatment groups and all measurements were conducted at the same time of the day (9:30a.m.-11:30a.m.). The leaf was placed into a custom-made single leaf chamber (chamber: polyoxymethylene, lid: poly (methyl methacrylate)), openings sealed with sponge rubber, which was connected to the LI-COR. Photosynthetic parameters were recorded after the reads were stable. We analyzed 9 diploid populations and 11 tetraploid populations. We observed an increased net photosynthetic rate in tetraploids in both control and drought conditions. We note large population-specific variation in both cytotypes.

Data were analyzed using R Version 3.6.0 (2019-04-26) with RStudio Version 1.2.1335. Data were plotted using the ggplot2 package version 3.2.1. The lsmeans package version 2.30–0 was used to fit a linear model to the data while the package bestNormalize version 1.4.3 was used for data normalization and estimation of normality. The package sjPlot version 2.8.2 was used to generate a summary table for the linear model fitted to the data. The package flextable version 0.5.9 was used to generate summary tables containing averages, sd and ci intervals.

Reference genome assembly and alignment

We generated a long read-based *de novo* genome assembly using Oxford Nanopore and Hi-C approaches, below.

High molecular weight DNA isolation and Oxford Nanopore sequencing

A total of 0.4 g *Cochlearia excelsa* leaf material from one individual plant was ground using liquid nitrogen before the addition of 10 mL of CTAB DNA extraction buffer (100 mM Tris-HCl, 2% CTAB, 1.4 M NaCl, 20 mM EDTA, and 0.004 mg/mL Proteinase K). The mixture was incubated at 55°C for 1 h then cooled on ice before the addition of 5 mL Chloroform. This was then centrifuged at 3500 *x g* for 30 min and the upper phase taken, this was added to 1X volume of phenol:chloroform:isoamyl-alcohol and spun for 30 min at 3500 *x g*. Again, the upper phase was taken and mixed with a 10% volume of 3M NaOAc and 2.5X volume of 100% ethanol at 4°C. This was incubated on ice for 30 min before being centrifuged for 30 min at 3500 *x g* and 4°C. Three times the pellet was washed in 4mL 70% ethanol at 4°C before being centrifuged again for 10 min at 3500 *x g* and 4°C. The pellet was then air dried and resuspended in 300 μL nuclease-free water containing 0.0036 mg/mL RNase A. The quantity and quality of high molecular weight DNA was checked on a Qubit Fluorometer 2.0 (Invitrogen) using the Qubit dsDNA HS Assay kit. Fragment sizes were assessed using a Q-card (OpGen Argus) and the Genomic DNA Tapestation assay (Agilent). Removal of short DNA fragments and final purification to HMW DNA was performed with the Circulomics Short Read Eliminator XS kit.

Long read libraries were prepared using the Genomic DNA by Ligation kit (SQK-LSK109; Oxford Nanopore Technologies) following the manufacturer's procedure. Libraries were then loaded onto an R9.4.1 PromethION Flow Cell (Oxford Nanopore Technologies) and run on a PromethION Beta sequencer. Due to the rapid accumulation of blocked flow cell pores or due to apparent read length anomalies on some *Cochlearia* runs, flow cells used in runs were treated with a nuclease flush to digest blocking DNA fragments before loading with fresh library according to the Oxford Nanopore Technologies Nuclease Flush protocol, version NFL_9076_v109_revD_08Oct2018.

Genome size estimation and computational ploidy inference

We used KMC[124] to create a k-mer frequency spectrum (Kmer length = 21) of trimmed Illumina reads. We then used GenomeScope 2.0 (parameters: -k 21 -m 61) and Smudgeplot[42] to estimate genome size and heterozygosity from k-mer spectra. To ensure robust results free of PCR artifacts, we PE150 Illumina sequenced one *C. officinalis* individual, ROT 20, to 120x coverage after library preparation with PCR-free Illumina library construction. A preponderance of simplex genotypes (AAAB) over duplex (AABB) genotypes indicated autotetraploidy over allotetraploidy in *C. officinalis*.

Data processing and assembly

Fast5 sequences produced by PromethION sequencing were base called using the Guppy 6 high accuracy base calling model (dna_r9.4.1_450bps_hac.cfg) and the resulting fastq files were quality filtered by the base caller. A total of 17.2 GB base called data were generated for the primary assembly, resulting in 60x expected coverage. Primary assembly was performed in Flye[38] and Necat.[39] The contigs were polished to improve the single-base accuracy in a single round of polishing in Medaka[125] and Pilon.[126]

Pseudomolecule construction by Hi-C, assembly cleanup, and polishing

To scaffold the assembled contigs into pseudomolecules, we performed chromosome conformation capture using Hi-C. Leaves from a single plant were snap-frozen in liquid N and ground to a fine powder using mortar and pestle. The sample was then homogenized, cross-linked and shipped to Phase Genomics (Seattle, USA), who prepared and sequenced an *in vivo* Hi-C library. After filtering low-quality reads with Trimmomatic,[127] we aligned the Hi-C reads against the contig-level assembly using bwa-mem[128] (settings −5 -S -P) and removed PCR duplicated using Picard Tools (https://broadinstitute.github.io/picard/). We used 3D-DNA[129] to conduct the initial scaffolding, followed by a manual curation in Juicebox.[130] After manually assigning chromosome boundaries, we searched for centromeric and telomeric repeats to orient the chromosome arms and to assess the completeness of the assembled pseudomolecules. To identify the centromeric repeat motif in *C. excelsa*, we used the RepeatExplorer[131] pipeline to search for repetitive elements from short-read sequence data originating from the reference individual. RepeatExplorer discovered a highly abundant 102 nucleotide repeat element (comprising 21% of the short-read sequence), which we confirmed as the centromeric repeat motif by fluorescence *in situ* hybridisation. Using BLAST, we localised the centromeric and telomeric (TTTAGGG) repeats and used them to orient the chromosome arms. We performed a final assembly cleanup in Blobtools[40] (Figure S1A). Gene space completeness was assessed using BUSCO version 3.0.2[43] and Compleasm.[44] Assembly completeness was assessed with Merqury and Meryl[41] with default settings.

Assembly annotation and RNA-seq

Prior to gene annotation, we identified and masked transposable element (TE) sequences from the genome assembly. To do so, we used the EDTA pipeline,[132] which combines multiple methods to comprehensively identify both retrotransposons and DNA transposons. After running EDTA on our chromosome-level genome assembly, we performed BLAST queries against a curated protein database from Swiss-Prot to remove putative gene sequences from the TE library and masked the remaining sequences from the assembly using RepeatMasker (https://www.repeatmasker.org).

We then used the BRAKER2[45] pipeline to conduct gene annotation on the TE-masked genome assembly. Evidence types included RNA-seq data from the identical *C. excelsa* line and protein data from related species. RNA-seq was generated from bud, stem and leaf tissue. Total RNA was extracted from each tissue using the Qiagen RNeasy Extraction Kit. Stranded RNA libraries with polyA were constructed Using NEB Next Ultra II Directional RNA Library Prep Kit for Illumina and then evaluated by qPCR, TapeStation

and Qubit at the DeepSeq facility (Nottingham, UK) before being sequenced at PE 150 at Novogene, inc (Cambridge, UK). We mapped the RNA-seq reads of each tissue to our reference genome using STAR[133] with default parameters (-twopassMode Basic) before running BRAKER2. Running BRAKER2 without UTR prediction generated more gene models and much better BUSCO metrics than with UTR prediction (97.8% [raw, pre-Blobtools trimmed] complete BUSCOs without UTR prediction vs. 91.7% with UTR prediction), so for the final annotation, we used the more complete set and ran BRAKER2 without UTR prediction.

Population resequencing and analysis

Library preparation and sequencing

DNA was prepared using the DNeasy Plant Mini Kit from Qiagen. DNA libraries were made using TruSeq DNA PCR-free Library kit from Illumina as per the manufacturer's instructions and were multiplexed based on concentrations measured with a Qubit Flourometer 2.0 (Invitrogen) using the Qubit dsDNA HS Assay kit. Sequencing was carried out on either NextSeq 550 (Illumina) in house (4 runs) or sent to Novogene for Illumina Hiseq X, PE150 sequencing (2 runs).

Data preparation, alignment, and genotyping

Reads were quality trimmed with Trimmomatic 0.39[127] (PE -phred33 LEADING:10 TRAILING:10 SLIDINGWINDOW:4:15 MINLEN:50) and then aligned to the *C. excelsa* reference using bwa-mem[134] and further processed with Samtools.[135] Duplicate reads were removed and read group IDs added to the bam files using Picard (version 1.134). Indels were realigned with GATK (version 4.2.3.0).[136] Samples were first genotyped individually with "HaplotypeCaller" (–emit-ref-confidence BP_RESOLUTION –minbase-quality-score 25 –minimum-mapping-quality 25) and were then genotyped jointly using "GenotypeGVCFs" in GATK (version 4.2.3.0). The resulting VCF files were then filtered for bi-allelic sites and mapping quality (QD < 2.0, FS > 60.0, MQ < 40.0, MQRankSum < −12.5, ReadPosRankSum < −8.0, HaplotypeScore <13.0). The VCF was then filtered by depth to avoid mapping artifacts based on common structural variants. Following Monnahan et al.[48] we further removed SNPs with per-sample sequencing depth >1.6x the mean depth to avoid issues caused by paralogous mapping.

Demographic analysis

We used a well-established[18,23,46–48] polyploid-specific pipeline to perform appropriate demographic analyses (principles elaborated in[46]). We first inferred genetic relationships between individuals using principal component analysis (PCA). Following,[137] we estimated a matrix of genetic covariances between each pair of individuals. For two individuals, *i* and *j*, covariance (*C*) was calculated as:

$$C_{ij} = \frac{1}{m}\sum_{s=1}^{m}\frac{(g_{is}/x_i - p_s)(g_{js}/x_j - p_s)}{p_s(1-p_s)},$$

where *m* is the number of variable sites, g_{is} is the genotype of individual *i* in site *s*, *x* is the ploidal level of the individual, and *p* is the alternate allele frequency. PCA was performed on the matrix using the R function *prcomp*, setting scaling to TRUE, and the first two axes of the rotated data extracted for plotting (https://github.com/thamala/polySV). For fastSTRUCTURE we followed[48] by randomly subsampling two alleles from tetraploid and hexaploid individuals using a custom script. We have previously demonstrated that results generated in this way are directly comparable to results generated with the full dataset in STRUCTURE.[48] To determine optimal K, model complexity that maximizes marginal likelihood and model components used to explain structure in data were determined using the approach included in the fastSTRUCTURE software (chooseK.py; https://github.com/rajanil/fastStructure). We calculated Nei's distances among all individuals in StAMPP[138] and visualized these using SplitsTree.[139] Linkage disequilibrium was estimated using ldsep.[140] To avoid biasing the estimates with unequal sample sizes, we chose 39 diploids and tetraploids for the analysis. To reduce computation time, the analysis was performed on 4-fold sites from a single chromosome (chromosome 1). To visualize the decay of LD as a function of physical distance, we calculated the average r^2 in 10 bp non-overlapping windows and fit a loess curve on the binned data.

Window-based scan for selective sweep signatures

We performed a window-based divergence scan for selection consisting of 1 kb windows that contained at least 15 SNPs. The data were filtered as described above and in addition was filtered for no more than 20% missing data and a depth of $\geq$ 8x. We calculated the following metrics: Rho,[52] Nei's F_{ST},[54] Weir-Cochran's F_{ST},[55] Hudson's F_{ST},[53] Dxy,[51] number of fixed differences and average groupwise allele frequency difference (AFD). To determine the best metric to detect localized peaks of divergence we performed a quantitative analysis of AFD plot quality for all 1% outliers of each metric. Each window was given a score of 0–4, with 0 being the lowest quality and 4 the highest. Scores were based on two qualities: peak height and peak specificity. For peak height one point was awarded if the window contained one SNP of AFD between 0.5 and 0.7, and two points were awarded for any SNP of AFD >0.7. Likewise, for peak specificity two points were awarded for an AFD peak that was restricted to a single gene and one point was awarded for a peak that was restricted to 2–3 genes. Compared to all other single 1% outlier lists and all permutations of overlapped 1% outlier lists, the top 1% outliers from Hudson's F_{ST} performed most favorably as it maximized the number of '4' and '3' scores while minimizing the number of '1' and '0' scores. Finally, we masked from the downstream analysis a region of uniformly high differentiation marking an inversion at scaffold 6 (between 5,890,246 and 6,137,362 bp).

MAV analysis

Following,[18] we performed a FineMAV[76]-like analysis on all bi-allelic, non-synonymous SNPs passing the same filters as the window-based selection scan. SNPs were assigned a Grantham score according to the amino acid change and this was scaled by the AFD

between ploidies. SNPs were first filtered for a minimum AFD of 0.25. The top 1% outliers of all these MAV-SNPs were then overlapped with the genes in our 1% F_{ST} outlier windows to give a refined list of candidate genes that contain potentially functionally significant non-synonymous mutations at high AFD between cytotypes. The code outlining this can be found at https://github.com/paajanen/meiosis_protein_evolution/tree/master/FAAD.

Orthogrouping and reciprocal best blast hits

We performed an orthogroup analysis using Orthofinder version 2.5.5.[113] to infer orthologous groups (OGs) from four species (*C. amara, A. lyrata, A. thaliana, C. excelsa*). A total of 25,199 OGs were found. Best reciprocal blast hits (RBHs) for *Cochlearia* and *A. thaliana* genes were found using BLAST version 2.9.0. *Cochlearia* genes were then assigned an *A. thaliana* gene ID for GO enrichment analysis in one of five ways. First if the genes' OG contained only one *A. thaliana* gene ID, that gene ID was used. If the OG contained more than one *A. thaliana* gene ID then the RBH was taken. If there was no RBH then the OG gene with the lowest E-value in a BLAST versus the TAIR10 database was taken. If no OG contained the *Cochlearia* gene then the RBH was taken. Finally, if there was no OG or RBH then the gene with the lowest E-value in a BLAST versus the TAIR10 database was taken. BLASTs were performed using the TAIR10.1 genome with data generated on 2023-01-02. To test of overlap is greater than expected by chance, we used the SuperExactTest.[115] This test implements a theoretical framework for computing the statistical distributions of multi-set intersections, by which it can then calculate the exact probability of multi-set intersections.

GO enrichment analysis

To infer functions significantly associated with directional selection following WGD, we performed gene ontology enrichment of candidate genes in the R package TopGO v.2.52,[141] using our *Cochlearia* universe set. We tested for overrepresented Gene Ontology (GO) terms within the three domains Biological Process (BP), Cellular Component (CC) and Molecular Function (MF) using Fisher's exact test with the conservative 'elim' method, which tests for enrichment of terms from the bottom of the hierarchy to the top and discards any genes that are significantly enriched in a descendant GO term. We used a significance cut-off of 0.05.

GO overlap significance

A permutation test was performed to determine whether the number of overlaps between GO categories observed was likely to occur by chance. For each species a list of random genes with the same size as the real candidate gene list was generated using all the genes that could appear in the selection scan (i.e., in windows that pass quality controls). GO analyses were then performed on these random lists and the number of overlapping GO categories was determined. This was performed 10,000 times. *p*-values were calculated as the proportion of randomized repeats where an equal or greater number of overlapping GO terms were discovered compared to the observed data.

Generation of consensus sequences

Consensus sequences were generated for proteins of interest so that they could be closely inspected via multiple sequence alignments and 3D protein structure prediction. Genomic regions were selected for either all diploids or all tetraploids present in the selection scan with GATK SelectVariants, while simultaneously being filtered for bi-allelic SNPs, ''–max-nocall-fraction 0.2'' and ''-select 'AF > 0.5'''. A consensus sequence was generated for exons by combining samtools faidx and bcftools consensus. Finally, a VCF containing only non-biallelic variation was manually inspected and any multiallelic variants at AF>0.5 and max-no-call-fraction<0.2 were manually incorporated into the consensus.

Multiple sequence alignments (MSAs)

We generated multiple sequence alignments using Clustal-Omega[142] in combination with amino acid sequences from the GenBank database. Sequences were selected either because the genes/proteins were well studied in other organisms or to give a phylogenetically broad coverage. Alignments were manually refined and visualized in JalView.[143]

Protein modeling

Protein homology models were created using AlphaFold[144] version 2.1 on the Czech national HPC MetaCentrum. The full database was used with a model preset of monomer and a maximum template data of 2020-05-14. Structures were visualized and images were generated in the PyMOL Molecular Graphics System (Version 2.0 Schrödinger, LLC).

QUANTIFICATION AND STATISTICAL ANALYSIS

Quantification and statistical analysis

Statistical significance threshold was defined as: $p < 0.05$ (*); $p < 0.01$ (**); and $p < 0.001$ (***) throughout the study.

HEI10 foci were counted at pachytene using NIS software and *p*-values for a significant per-bivalent reduction in class I mature crossovers was established using the Mann-Whitney U test (Minitab v 18.1.0.0).

Significance in the salinity tolerance experiments was tested with the Wilcoxon rank-sum test with continuity correction performed in R Version 3.6.0.

p-values for drought tolerance, stomatal conductance and photosynthetic rate were assessed using R Version 3.6.0 (2019-04-26) with RStudio Version 1.2.1335. Averages, standard deviation and confidence interval for relative stomatal conductance and net photosynthesis can be found in Tables S5–S7. The lsmeans package version 2.30–0 was used to fit a linear model to the data while the package bestNormalize version 1.4.3 was used for data normalization and estimation of normality. The package sjPlot version 2.8.2 was used to generate a summary table for the linear model fitted to the data. The package flextable version 0.5.9 was used to generate summary tables containing averages, sd and ci intervals.

Elevated Dxy values in the most extreme 25 Fst outliers was tested with a Mann Whitney U test performed in R Version 3.6.0.

Significant overlap between candidate gene homologues was calculated using a SuperExactTest[72] performed in R Version 3.6.0. This test implements a theoretical framework for computing the statistical distributions of multi-set intersections, by which it can then calculate the exact probability of multi-set intersections.

A permutation test was performed to determine whether the number of overlaps between GO categories was significant. Bespoke python code was used to generate random gene lists (same size as the real candidate gene lists), perform GO analysis on and count the number of overlaps 10,000 times. *p*-values were calculated as the proportion of randomized repeats where an equal or greater number of overlapping GO terms were discovered compared to the real data.

Overrepresented Gene Ontology (GO) terms within the three domains Biological Process (BP), Cellular Component (CC) and Molecular Function (MF) was determined in R Version 3.6.0 using Fisher's exact test with the conservative 'elim' method, which tests for enrichment of terms from the bottom of the hierarchy to the top and discards any genes that are significantly enriched in a descendant GO term.

Cell Reports, Volume *43*

Supplemental information

Kinetochore and ionomic adaptation to whole-genome duplication in *Cochlearia* shows evolutionary convergence in three autopolyploids

Sian M. Bray, Tuomas Hämälä, Min Zhou, Silvia Busoms, Sina Fischer, Stuart D. Desjardins, Terezie Mandáková, Chris Moore, Thomas C. Mathers, Laura Cowan, Patrick Monnahan, Jordan Koch, Eva M. Wolf, Martin A. Lysak, Filip Kolar, James D. Higgins, Marcus A. Koch, and Levi Yant

Supplemental Figures

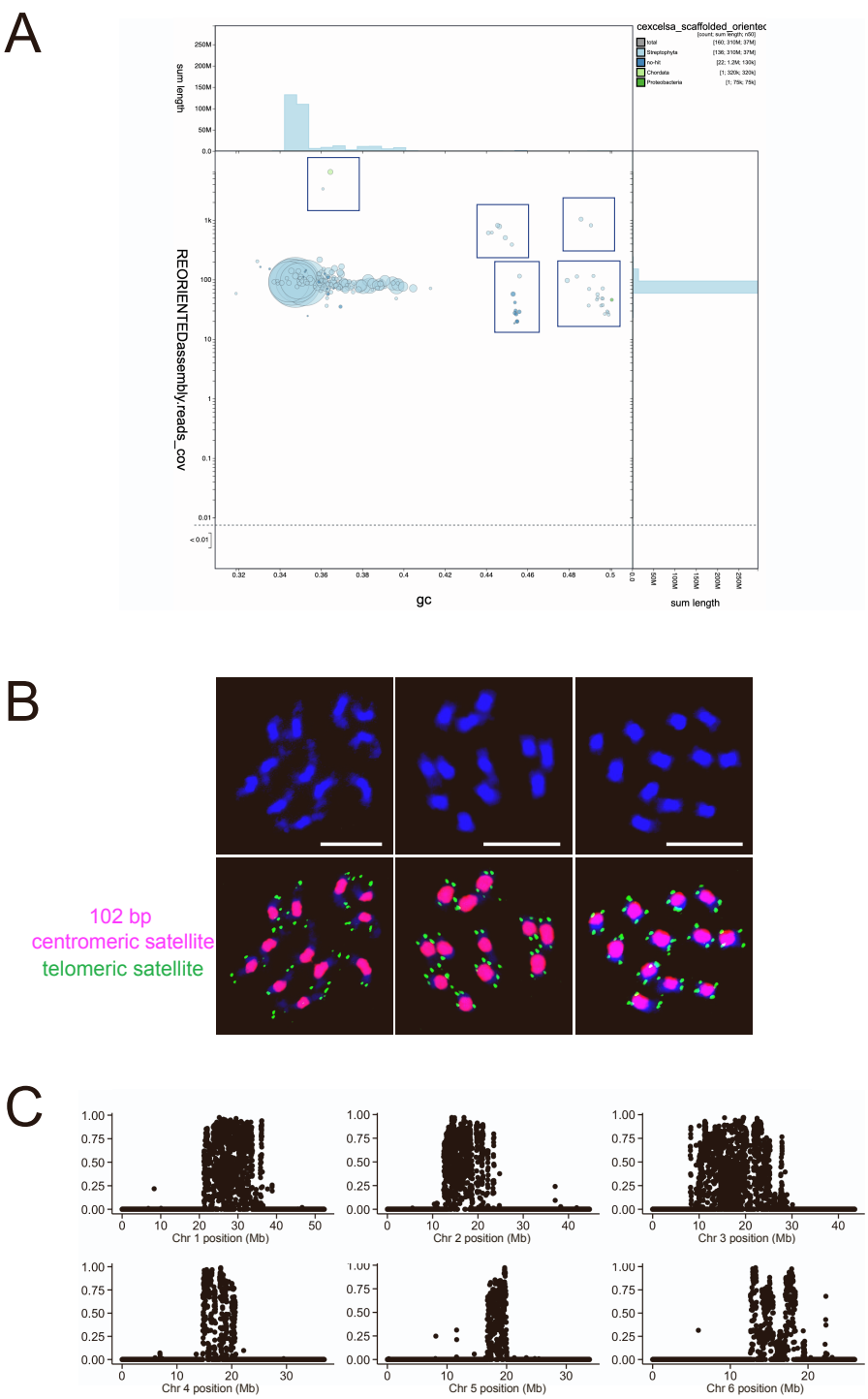

Figure S1. *Cochlearia excelsa* genome assembly clean-up, fluorescent *in situ* hybridization and repeat mapping. Related to Figure 1. (**A**) Final filtering of contaminant contigs with Blobtools. Rectangles indicate contigs flagged as contamination or organellar based on GC content (x-axis), outlier read depth (y-axis), and homology in the UniProt database (colours, in key insert top right; see methods). The final assembly (at https://doi.org/10.5061/dryad.ncjsxkt1s) consists of 121 scaffolds, 6 of which comprise of telomere-to-telomere sequences representing the 6 *C. excelsa* base chromosomes and were used in this study as reference. The remaining 115 small contigs are included in the assembly and were used in initial read mapping, but were excluded from downstream analysis, because they contain 0% BUSCOS and largely comprise of masked repeat sequences (>82% of bases in the 115 small contigs are masked repeats). (**B**) Metaphase chromosomes (2n = 12; top) were subjected to hybridization using 102 bp satellite (pink) and *Arabidopsis*-type telomeric satellite (green) probes hybridizing to all (peri)centromeres and telomeres, respectively (bottom). Chromosomes were counterstained with DAPI. Scale bar, 10 μm; (**C**) Mapping of simple 102 bp centromeric repeat, comprising a substantial 21% of genomic sequence.

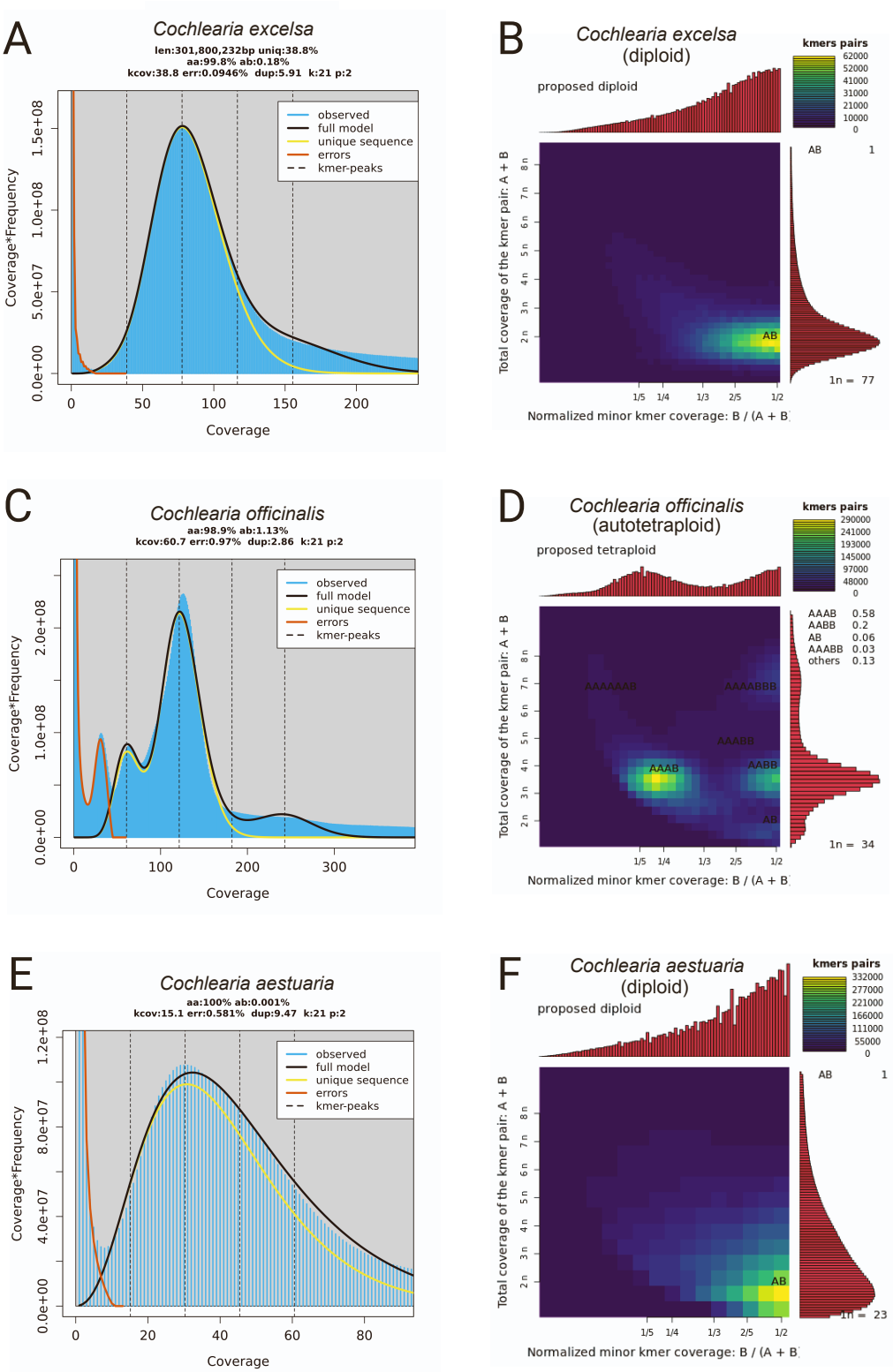

Figure S2. Ploidy assessments of three key *Cochlearia* species. Related to Figure 1. (**A, C, E**) GenomeScope and (**B, D F**) Smudgeplot profiles estimating ploidy. (**A**) Reference *C. excelsa* genome size of 302 mb with low heterozygosity, (**B**) confirmed diploid. (**C, D**) *C. officinalis* focal autotetraploid used in the genome scans. The preponderance of simplex genotypes (AAAB) over duplex (AABB) kmer proportions indicate autotetraploidy over allotetraploidy in *C. officinalis*. (E, F) *C. aestuaria* population VEG confirmed diploid with unusually high homozygosity.

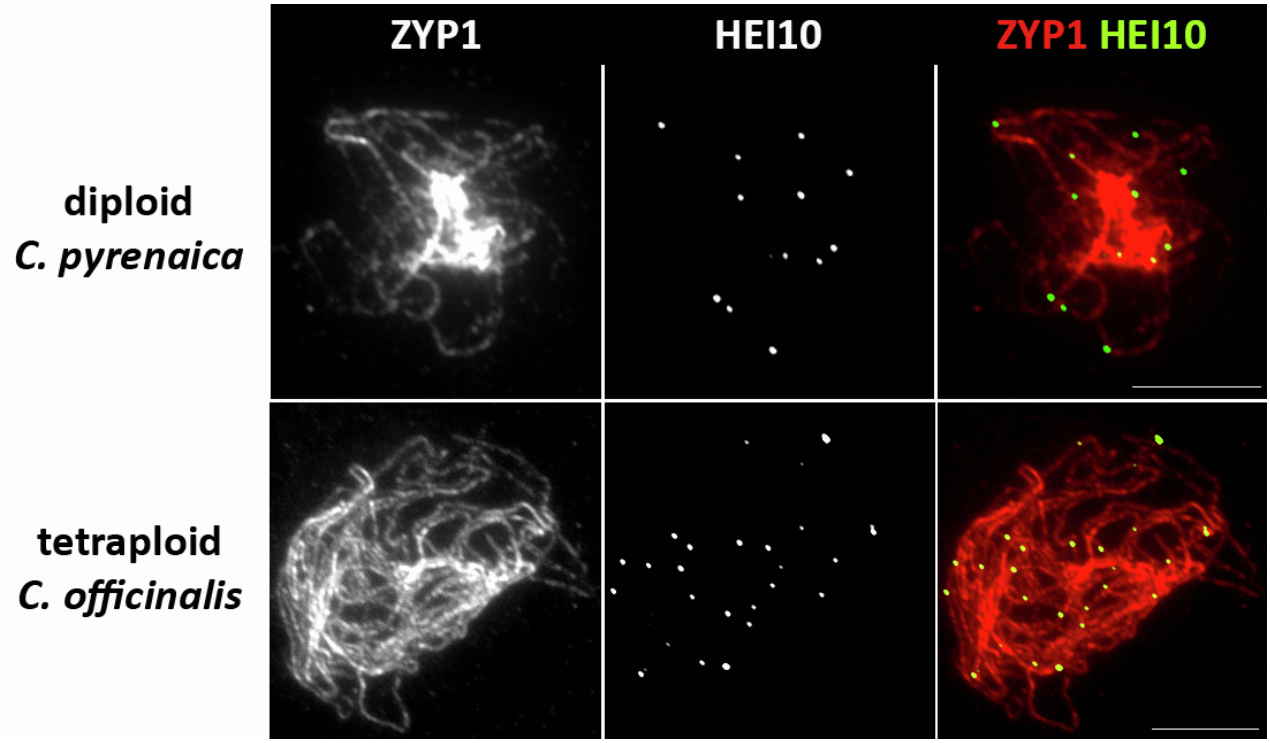

Figure S3. HEI10 foci per bivalent are reduced in tetraploid vs diploids. Related to Figure 2. Representative pachytene nuclei immunostained with ZYP1 and HEI10. Signal is split into separate channels per panel to more clearly show that all HEI10 foci are chromosome-associated. Scale bars = 10μm.

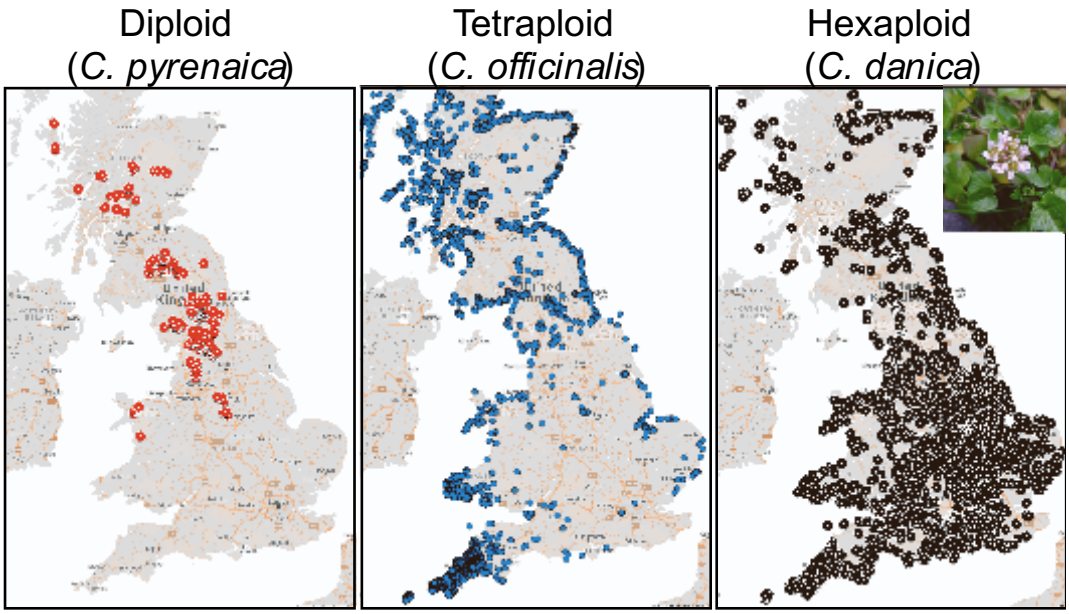

Figure S4. Contrasting distributions of major *Cochlearia* cytotypes. Related to Figure 1 and 3. Left: Diploids deeply inland in nonsaline habitats; Centre; tetraploids inhabiting coastal regions; Right: *Cochlearia danica*, the hexaploid, exclusively coastal until the 1970's, has explosively invaded salted motorways since the practice of salting the roads began at that time. Data: complete download of reported botanical observations from the records of the Botanical Society of Britain & Ireland (1895-2021).

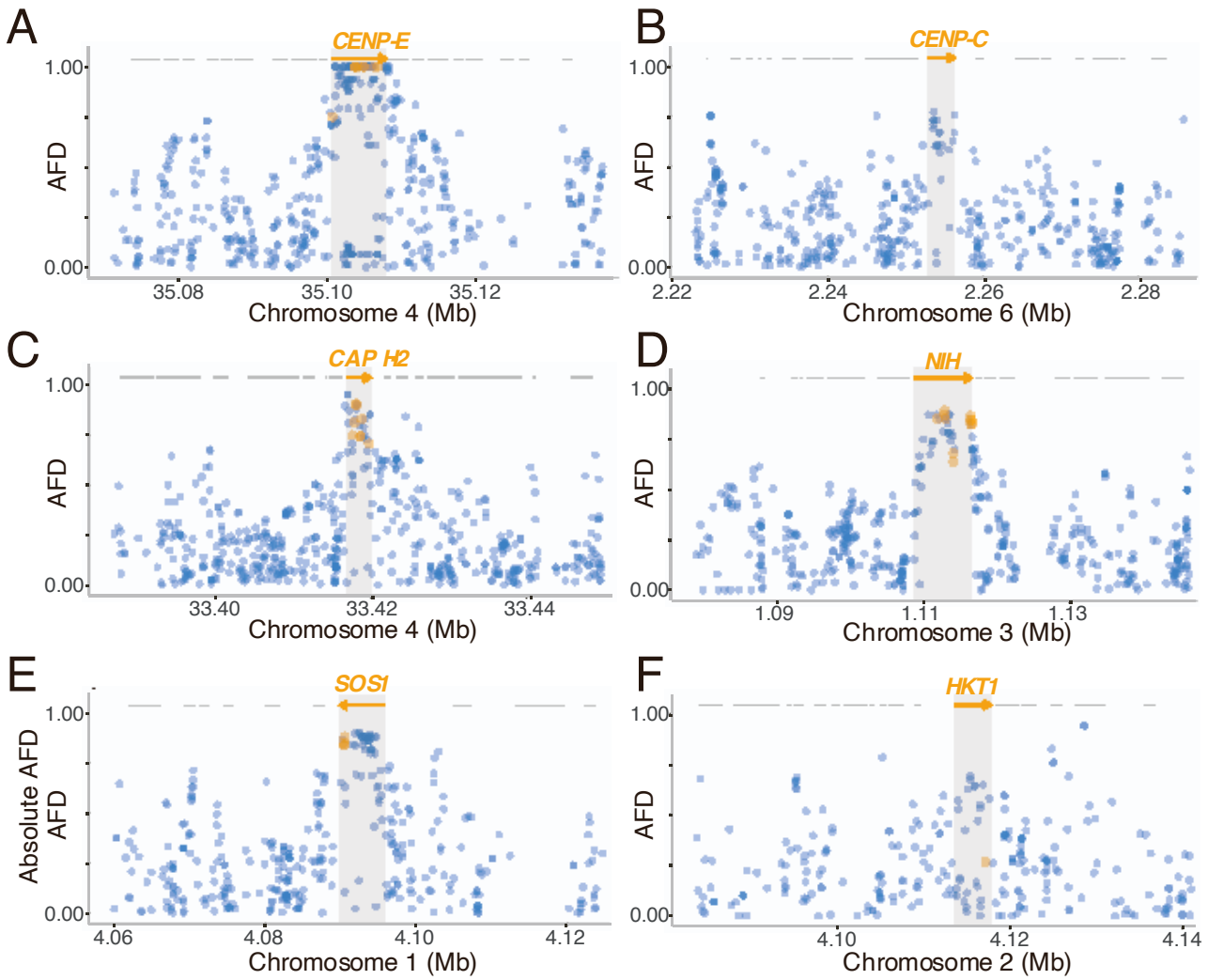

Figure S5. Top selective sweep signatures are robust to ecotype and differentiate purely by ploidy. Related to Figure 5. The same 6 outlier genes shown in Fig. 5, here assessed with only inland (non-salt ecotype) tetraploids vs diploids of similar inland freshwater spring environments. (**A-D**) Represent kinetochore or DNA management; (**E-F**) ion homeostasis functional categories. The X axis gives genome position in megabases (Mb). The Y axis gives Allele Frequency Differences by ploidy at single SNPs (dots) between diploid and tetraploid *Cochlearia*. Orange arrows indicate genes overlapping the top FST gene outliers, and grey lines indicate neighbouring genes. Orange dots indicate MAV outliers.

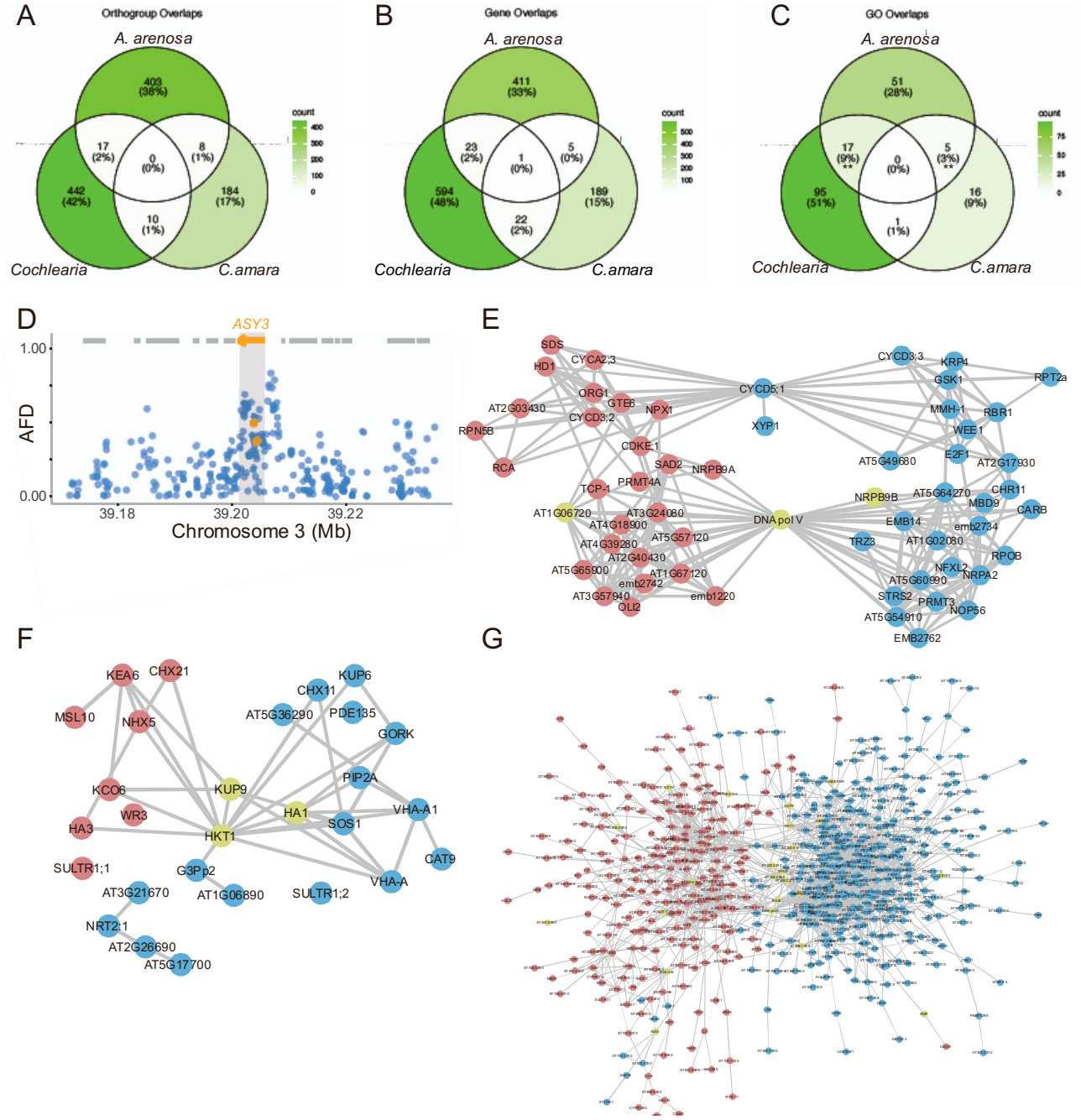

Figure S6. Greater process-level than gene-level convergence. Related to Figure 5. **(A-C)** Overlaps of *Cochlearia, A. arenosa,* and *C. amara* selective sweep candidates. A modest degree of process-level convergence (panel **A**) is evident between *Cochlearia* and *A. arenosa*. A lack of enrichment for gene-level convergence is seen either by the orthogrouping (Panel **B**) or nearest homolog (Panel **C**) approaches. **(D)** Evidence of selective sweep at *ASY3* in *Cochlearia* autotetraploids**.** The ortholog of this gene is functionally validated to have a primary role in stabilizing autotetraploid meiosis in *A. arenosa* and is also in our 1% FST outlier list in *Cochlearia*. X axis=genome position in megabases (Mb). Y axis=allele Frequency Differences by ploidy at single SNPs (dots) between diploid and tetraploid *Cochlearia*. Orange arrows indicate genes overlapping the top FST gene outliers, and grey lines indicate neighbouring genes. Orange dots indicate MAV outliers. **(E-G)** Evidence for functional convergence between *Cochlearia* and *Arabidopsis arenosa* following independent WGDs. STRING plots show *Cochlearia* candidate genes (blue) and *A. arenosa* candidate genes (red). Convergent genes that are present in both species' outlier lists as selection candidates are in yellow. **(E)** A large shared cluster surrounding the endopolyploidy gene *CYCD5;1*, which has many connections to large cluster centring on *DNA pol V*, which is an outlier in both datasets; **(F)** ion transport-related genes with a highly interconnected cluster of top outliers in both genome scans, *HKT1, KUP9,* and *HA1;* **(G)** The entire set of candidates in both genome scans for which the STRING database has information.

Supplemental Tables

Table S1. Overall summary metrics of *Cochlearia excelsa* genome assembly

Assembly characteristic	Value
Number of scaffolds	121
Total scaffold length (bp)	310,488,619
Scaffold N50 (bp)	36,866,022
Largest scaffold (bp)	52,330,213
N50 (bp)	36,866,022
N90 (bp)	1,360,602
auN (bp)	32,000,305
L50	4
L90	25
GC content (%)	35
Percent complete BUSCO genes	97.67

Note: Compleasm was used to calculate BUSCOs using the using the *brassicales_odb10* lineage (n=4596). Related to Figure 1.

Table S2. Repeat and completeness metrics of the *Cochlearia excelsa* scaffolds

Chromosome	Length (bp)	% repeats	Genome completeness
1	52,330,213	N/A	N/A
2	44,613,338	N/A	N/A
3	43,484,660	N/A	N/A
4	36,866,022	N/A	N/A
5	33,887,346	N/A	N/A
6	26,002,966	N/A	N/A
1-6	237,184,545	40.7%	94.4%
(debris contigs)	73,304,074	83.1%	2.9%
Total	310,488,619	55.6%	97.3%

Note: Table shows that debris contigs are very repeat rich and contribute proportionally to genome completeness, indicating they are comprise primarily uncollapsed repeats, consistent with HiC trans interactions with centromere repeats (Fig. 1B) and no contribution to BUSCOs. Genome completeness was calculated with Merqury. Related to Figure 1.

Table S3. Chromosome stability scoring of individual diploid and autotetraploid *Cochlearia* plants at meiotic metaphase I.

Ploidy	Pop.	# scored spreads	# stable	% stable	# rather stable	% rather stable	# rather unstable	% rather unstable	# unstable	% unstable
2	LAB_201	28	18	64.3	10	35.7	0	0	0	0
2	LAB_210	26	9	34.6	10	38.5	4	15.4	3	11.5
2	NEN_201	24	12	50.0	9	37.5	2	8.3	1	4.2
2	NEN_202	12	3	25.0	5	41.7	1	8.3	3	25.0
2	NEN_203	17	5	29.4	7	41.2	2	11.8	3	17.6
2	NEN_204	22	13	59.1	9	40.9	0	0	0	0
2	NEN_205	11	5	45.5	4	36.4	0	0	2	18.2
2	NEN_206	22	7	31.8	11	50.0	3	13.6	1	4.5
2	NEN_207	12	4	33.3	4	33.3	4	33.3	0	0
2	NEN_208	12	6	50.0	4	33.3	2	16.7	0	0
2	NEN_209	32	24	75.0	6	18.8	2	6.3	0	0
2	NEN_211	16	3	18.8	6	37.5	4	25.0	3	18.8
2	NEN_212	15	7	46.7	8	53.3	0	0	0	0
2	Average			**43.3**		**38.3**		**11**		**8**
4	ROT_201	17	2	11.8	12	70.6	1	5.9	2	11.8
4	ROT_204	11	0	0	0	0	0	0	11	100.0
4	ROT_205	45	0	0	18	40.0	16	35.6	11	24.4
4	ROT_208	17	0	0	5	29.4	8	47.1	4	23.5
4	ROT_210	5	0	0	0	0	2	40.0	3	60.0
4	SKN_201	19	0	0	14	73.7	5	26.3	0	0
4	SKN_202	15	0	0	6	40.0	4	26.7	5	33.3
4	SKN_207	33	1	3.0	13	39.4	18	54.5	1	3.0
4	SKN_209	12	0	0	0	0	4	33.3	8	66.7
4	SKN_210	19	0	0	4	21.1	8	42.1	7	36.8
4	SKN_211	29	0	0	10	34.5	17	58.6	1	3.4
4	Average			**1.3**		**31.7**		**34**		**33**

Note: In diploids, chromosome spreads with 6 bivalents were scored as "stable meiosis", 5-4 as "rather stable", 3 as "rather unstable", and <3 as "unstable". In tetraploids, chromosome spreads with 12 bivalents were scored as "stable meiosis", 11-9 as "rather stable", 8-6 as "rather unstable", and <6 as "unstable". Related to Figure 2.

Table S4. Phenotype scores for *Cochlearia* plants following salt stress treatment.

Maternal Line	Scores	Average Score	Number of Samples	Standard Deviation	Ploidy
CHA_001	7, 5, 6, 7, 5, 7, 7, 4, 4, 3, 5, 8, 0, 0, 3	4.73	15	2.46	2x
CHA_010	5, 7, 5, 6, 4, 2, 3	4.57	7	1.72	2x
CHA_011	7, 4, 0, 4, 6, 6, 8, 7, 2, 2, 4, 5, 3	4.46	13	2.33	2x
CHA_002	4, 6, 6, 7, 5, 5, 6, 6	5.63	8	0.92	2x
CHA_008	7, 7, 8, 8, 8, 8, 7, 7, 9, 9, 7, 7, 9, 6, 9, 8, 6, 8, 8	7.68	19	0.95	2x
CWY_001	1	1.00	1	N/A	4x
CWY_013	3, 3, 3, 2, 2, 3, 2, 2, 5, 5, 5	3.18	11	1.25	4x
CWY_002	2	2.00	1	N/A	4x
CWY_003	3, 4, 5, 5, 2, 4, 3, 4, 4, 2, 3, 2, 1	3.23	13	1.24	4x
CWY_005	4, 3, 1, 2, 3, 2, 2, 3, 1, 1, 1	2.09	11	1.04	4x
LAB_002	5, 7, 7	6.33	3	1.15	2x
LAB_003	6, 4, 8, 6, 5, 5, 6, 8, 6, 5, 5, 4, 6, 2, 7, 4, 5, 2, 4, 7	5.25	20	1.65	2x
LAB_007	5, 6, 5, 7, 4, 6, 3, 6, 5, 3, 4, 4, 5, 5, 6, 6	5.00	16	1.15	2x
LAB_008	8, 6, 6, 7, 7, 7, 8, 8, 5, 7, 6, 8, 7, 6, 7, 7, 5, 7, 7, 7	6.80	20	0.89	2x
LAB_009	6, 5, 4, 5, 5, 5, 6, 7, 8, 5, 6, 5, 6, 5, 4, 5	5.44	16	1.03	2x
LAM_017	8, 6	7.00	2	1.41	2x
MAL_002	6, 7, 5, 6, 6, 7, 8, 6, 7, 5, 2, 0, 4, 6, 6, 7	5.50	16	2.03	2x
MAL_003	7, 8, 8, 5, 5, 5, 8, 8, 8, 5, 6, 9, 5	6.69	13	1.55	2x
MAL_004	7, 6, 6, 6, 4, 4, 6, 7, 6, 7, 7	6.00	11	1.10	2x
MAL_007	6, 5, 7, 6, 8, 6, 3, 4, 6, 6, 4, 6, 1, 3, 5	5.07	15	1.79	2x
NEN_002	1, 3, 2, 2, 3, 3, 3, 3, 1, 2, 1, 1, 2, 3, 3, 2, 3, 1, 2, 1	2.10	20	0.85	2x
NEN_003	7, 8, 8, 6, 6, 6, 7, 5, 8, 5, 4, 6, 8, 7, 0, 3, 7, 8, 5, 6	6.00	20	2.00	2x
NEN_004	2, 5, 7, 5, 4, 6, 7, 5, 5, 8, 8, 6, 6	5.69	13	1.65	2x
NEN_005	9, 6, 3, 7, 4, 6, 5, 7, 5, 8, 9, 6, 7, 3, 0, 4	5.56	16	2.39	2x
NEN_006	4, 6, 5, 6	5.25	4	0.96	2x
SCU_012	4, 3, 5, 4, 6, 4, 5, 4, 5, 5, 6, 7, 5, 5, 5, 5, 0, 5, 4, 7	4.70	20	1.49	4x
SCU_020	6, 7, 7, 7, 7, 7, 9, 7, 8, 6, 9, 10, 8, 9, 8, 8, 7, 9, 9	7.79	19	1.13	4x
SCU_003	4, 4, 3, 1	3.00	4	1.41	4x
SCU_009	3, 2, 3, 5	3.25	4	1.26	4x
TMN_001	3, 3, 4, 6, 3, 3, 5, 5, 4, 3, 2, 3, 0, 2, 3, 3, 2, 3, 4	3.21	19	1.32	4x
TMN_003	4, 5, 5, 5, 3, 3, 3, 2, 6, 3, 3, 5, 4, 4, 5, 4, 5, 7, 5, 4	4.25	20	1.21	4x
TMN_005	1, 5, 2, 1	2.25	4	1.89	4x
TMN_006	5, 4	4.50	2	0.71	4x
TYN_0H1	1, 4, 8, 5, 4, 2, 2, 2, 3, 2, 2, 1, 1, 3, 1, 2, 1, 2, 1, 1	2.40	20	1.76	2x
TYN_0H4	2, 3, 1, 3, 2, 1, 3, 1, 0, 1, 2, 4, 2, 1, 3, 2, 1, 2, 2, 0	1.80	20	1.06	2x
TYN_0H5	1, 3, 9, 7, 9, 8, 4, 0, 7, 8, 8, 8, 7, 6, 8, 9, 5, 5, 6, 5	6.15	20	2.58	2x
TYN_0H7	0, 5, 6, 6, 7, 5, 5, 4, 3, 0, 4, 6, 3, 2, 4, 5, 4, 2, 5, 3	3.95	20	1.90	2x
TYN_0H8	7, 6, 3, 4, 3, 3, 4, 5, 6, 6, 4, 5, 4, 3, 0, 1, 6, 5, 6, 6	4.35	20	1.81	2x
All diploids	N/A	4.98	367	1829.00	2x
All tetraploids	N/A	4.14	129	534.00	4x

Note: Averages, standard deviation and 95% confidence interval under control and drought stress are shown. Related to Figure 3.

Table S5. Net Photosynthetic rates under drought relative to control conditions.

relative net Photosynthesis							
Species	**Treatment**	**Ploidy**	**N**	**Average**	**sd**	**se**	**ci**
ELI21	Control	4x	4	**1.00**	0.12	0.06	0.19
ELI21	Drought	4x	5	**0.91**	0.10	0.04	0.12
ELI23	Control	4x	3	**1.00**	0.16	0.09	0.40
ELI23	Drought	4x	4	**0.78**	0.04	0.02	0.06
ELI25	Control	4x	5	**1.00**	0.22	0.10	0.27
ELI25	Drought	4x	3	**0.99**	0.09	0.05	0.22
ERS21+22	Control	4x	4	**1.00**	0.05	0.03	0.08
ERS21+22	Drought	4x	4	**1.04**	0.10	0.05	0.17
ERS23	Control	4x	3	**1.00**	0.19	0.11	0.48
ERS23	Drought	4x	4	**0.66**	0.04	0.02	0.07
ERS26	Control	4x	3	**1.00**	0.27	0.15	0.66
ERS26	Drought	4x	4	**0.83**	0.10	0.05	0.16
LAB22	Control	2x	5	**1.00**	0.25	0.11	0.31
LAB22	Drought	2x	5	**0.77**	0.11	0.05	0.14
LAB23	Control	2x	4	**1.00**	0.06	0.03	0.09
LAB23	Drought	2x	5	**0.60**	0.17	0.08	0.22
Nent20	Control	2x	3	**1.00**	0.03	0.02	0.08
Nent20	Drought	2x	7	**0.54**	0.14	0.05	0.13
Nent23	Control	2x	4	**1.00**	0.07	0.03	0.11
Nent23	Drought	2x	3	**0.48**	0.17	0.10	0.42
Nent24	Control	2x	4	**1.00**	0.32	0.16	0.51
Nent24	Drought	2x	6	**0.86**	0.12	0.05	0.12
PIT_020	Control	2x	13	**1.00**	0.14	0.04	0.09
PIT_020	Drought	2x	15	**0.82**	0.23	0.06	0.13
PIT_022	Control	2x	3	**1.00**	0.13	0.07	0.32
PIT_022	Drought	2x	3	**0.58**	0.08	0.05	0.20
PIT_023	Control	2x	3	**1.00**	0.03	0.02	0.08
PIT_023	Drought	2x	3	**0.84**	0.07	0.04	0.19
PIT_025	Control	2x	5	**1.00**	0.07	0.03	0.08
PIT_025	Drought	2x	5	**0.62**	0.04	0.02	0.05
SKN20	Control	4x	3	**1.00**	0.18	0.10	0.44
SKN20	Drought	4x	6	**0.65**	0.10	0.04	0.10
SKN21-A	Control	4x	6	**1.00**	0.16	0.07	0.17
SKN21-A	Drought	4x	6	**0.87**	0.20	0.08	0.21
SKN21-B	Control	4x	3	**1.00**	0.14	0.08	0.34
SKN21-B	Drought	4x	5	**0.93**	0.27	0.12	0.34
SKN24	Control	4x	5	**1.00**	0.12	0.06	0.15
SKN24	Drought	4x	5	**0.82**	0.16	0.07	0.20

Note: Averages, standard deviation and 95% confidence interval under control and drought stress are shown. Related to Figure 3.

Table S6. Stomatal conductance under drought relative to control conditions.

relative Stomata Conductance								
Species	**Treatment**	**Ploidy**	**N**	**Average**	**sd**	**se**	**ci**	**rn**
ELI21	Control	4x	4	**1.00**	0.15	0.08	0.24	1.00
ELI21	Drought	4x	5	**0.70**	0.20	0.09	0.24	0.70
ELI23	Control	4x	3	**1.00**	0.17	0.10	0.42	1.00
ELI23	Drought	4x	4	**0.98**	0.17	0.09	0.28	0.98
ELI25	Control	4x	5	**1.00**	0.20	0.09	0.24	1.00
ELI25	Drought	4x	3	**1.06**	0.95	0.55	2.37	1.06
ERS21+22	Control	4x	4	**1.00**	0.31	0.15	0.49	1.00
ERS21+22	Drought	4x	4	**0.62**	0.11	0.05	0.17	0.62
ERS23	Control	4x	3	**1.00**	0.39	0.22	0.97	1.00
ERS23	Drought	4x	4	**1.01**	0.50	0.25	0.79	1.01
ERS26	Control	4x	3	**1.00**	0.25	0.14	0.61	1.00
ERS26	Drought	4x	4	**1.44**	0.82	0.41	1.31	1.44
LAB22	Control	2x	5	**1.00**	0.48	0.21	0.60	1.00
LAB22	Drought	2x	5	**0.53**	0.24	0.11	0.30	0.53
LAB23	Control	2x	4	**1.00**	0.41	0.20	0.65	1.00
LAB23	Drought	2x	5	**0.39**	0.09	0.04	0.12	0.39
Nent20	Control	2x	3	**1.00**	0.00	0.00	0.01	1.00
Nent20	Drought	2x	7	**0.52**	0.18	0.07	0.16	0.52
Nent23	Control	2x	4	**1.00**	0.17	0.08	0.26	1.00
Nent23	Drought	2x	3	**0.54**	0.18	0.11	0.46	0.54
Nent24	Control	2x	4	**1.00**	0.27	0.13	0.43	1.00
Nent24	Drought	2x	6	**0.71**	0.18	0.07	0.19	0.71
PIT_020	Control	2x	13	**1.00**	0.23	0.06	0.14	1.00
PIT_020	Drought	2x	15	**0.81**	0.26	0.07	0.14	0.81
PIT_022	Control	2x	3	**1.00**	0.43	0.25	1.07	1.00
PIT_022	Drought	2x	3	**1.18**	0.05	0.03	0.12	1.18
PIT_023	Control	2x	3	**1.00**	0.37	0.21	0.92	1.00
PIT_023	Drought	2x	3	**0.71**	0.38	0.22	0.95	0.71
PIT_025	Control	2x	5	**1.00**	0.15	0.07	0.19	1.00
PIT_025	Drought	2x	5	**0.28**	0.04	0.02	0.05	0.28
SKN20	Control	4x	3	**1.00**	0.31	0.18	0.78	1.00
SKN20	Drought	4x	6	**0.70**	0.08	0.03	0.08	0.70
SKN21-A	Control	4x	6	**1.00**	0.38	0.15	0.40	1.00
SKN21-A	Drought	4x	6	**0.84**	0.36	0.15	0.37	0.84
SKN21-B	Control	4x	3	**1.00**	0.16	0.09	0.39	1.00
SKN21-B	Drought	4x	5	**0.91**	0.33	0.15	0.41	0.91
SKN24	Control	4x	5	**1.00**	0.12	0.05	0.14	1.00
SKN24	Drought	4x	5	**0.57**	0.13	0.06	0.16	0.57

Note: Averages, standard deviation and 95% confidence intervals under control and drought stress are shown. Related to Figure 3.

Table S7. Stomatal conductance and photosynthesis model results.

	Rel. Stomatal Conductance			**rel. Photosynthesis**		
Predictors	*Estimates*	*CI*	*p*	*Estimates*	*CI*	*p*
(Intercept)	-0.29	-0.55 – -0.03	**0.030**	-0.31	-0.57 – -0.05	**0.021**
Ploidy [4x]	0.62	0.24 – 1.00	**0.002**	0.66	0.28 – 1.04	**0.001**
Observations	98			98		
R^2 / R^2 adjusted	0.097 / 0.088			0.110 / 0.100		

Related to Figure 3.

Supplementary Data

Data S1. Supplemental Data tables S1 to S9.